PCCP

PAPER

View Article Online
View Journal

Published on 27 May 2015. Downloaded by University of California - San Diego on 02/06/2015 16:29:49.

Cite this: DOI: 10.1039/c5cp01405k

Colloidal properties and behaviors of 3 nm primary particles of detonation nanodiamonds in aqueous media†

N. O. Mchedlov-Petrossyan,*[a] N. N. Kamneva,[a] A. I. Marynin,[b] A. P. Kryshtal[c] and E. Ōsawa[d]

Received 10th March 2015,
Accepted 14th May 2015

DOI: 10.1039/c5cp01405k

www.rsc.org/pccp

This study was aimed to reveal the principal colloidal properties of the aqueous dispersion of extremely small primary single-crystalline diamond particles in water. Together with the non-diamond layer, the size of the colloidal species is 2.8 ± 0.6 nm as found *via* DLS of the initial 5.00 wt/vol% hydrosol. Anionic dyes are readily adsorbed on the colloidal species. This is in line with the positive zeta-potential. The critical coagulation concentrations of the 0.19 wt/vol% nanodiamond hydrosol were determined with a set of inorganic electrolytes and anionic surfactants. The data are in line with the Schulze–Hardy rule for "positive" sols. The fulfillment of the lyotropic (Hofmeister) series was also observed for single-charged anions. The abnormal influence of alkali gives evidence of the acidic nature of the positive charge of the nanodiamond species. Application of acid–base indicators allows estimating the value of the interfacial electrical potential of the nanodiamond particles. Upon dilution from 5.00% to 0.01%, the colloidal system under study exhibits unusual changes. The average size increases *ca.* ten-fold as determined by DLS. The TEM images support this observation. At the same time, the viscosity drops. This phenomenon was explained in terms of the so-called periodic colloidal structures (colloidal crystals) in concentrated solutions.

1. Introduction

In this paper, we report the colloid properties and behaviors of aqueous dispersion of 3 nm-sized detonation diamond species recently produced in the NanoCarbon Research Institute, Japan.

As the interest in nanodiamonds (NDs) increases rapidly from a variety of different fields of science and technology[1–6] it became desirable to discuss the state of dispersity in their particles. Especially tricky is the so-called detonation nanodiamonds, which are the smallest diamond particles available, and generally offered by many vendors as the source of primary particles 4–10 nm in diameter. People often use the commercial powder as received in the ill-belief that the visible aggregation can be easily destroyed by stirring in water or applying supersonic waves.[7] Neither of these techniques work.

In contrast to the optimistic view, the primary particles of detonation nanodiamonds have very strong tendency to aggregate by interfacial Coulombic interactions into hard agglomerates. Recently, the following concept of the interactions of ND primary species has been developed.[8] In the beginning of aggregation, interfacial interactions may not necessarily be optimal to give Incoherent Interfacial Coulombic Interactions (IICIs), but, given enough time and high temperature, the interfacial configurations in the agglomerates could rearrange into more tight ones due to Coherent Interfacial Coulombic Interactions (CICIs), which is comparable in bonding energies to covalent C–C bonds.[8] Detonation nanodiamonds as produced are supposed to consist mainly of CICI agglomerates. Attrition milling of aqueous suspension of crude detonation nanodiamonds provides, when performed under optimum conditions, a black colloidal solution of perfectly disintegrated primary particles;[9] some alternative methods for producing de-agglomerated nanodiamonds have also been described in detail.[10] This aqueous solution of colloidal nanocrystals is kinetically stable, but dilution often leads to its aggregation.

[a] Department of Physical Chemistry, Kharkov V. N. Karazin National University, Kharkov, 61022, Ukraine. E-mail: mchedlov@yandex.ru
[b] National University of Food Technologies, Volodymyrskaya, 68, Kiev, 01601, Ukraine
[c] Department of Physics and Technology, Kharkov V. N. Karazin National University, Kharkov, 61022, Ukraine
[d] NanoCarbon Research Institute, Ltd, AREC (Asama Research Extension Center), Faculty of Textile Science and Technology, Shinshu University, 3-15-1 Tokida, Ueda, Nagano 386-8567, Japan

† Electronic supplementary information (ESI) available: Conductivities and pH values of ND hydrosols of different concentrations, the IR and EDX spectra of the solid samples obtained from the ND hydrosols, the absorption spectra of dyes in the presence of ND nanoparticles, data concerning the coagulation by electrolytes, transmission electron microscopy images, and some other details. See DOI: 10.1039/c5cp01405k

Published on 27 May 2015. Downloaded by University of California - San Diego on 02/06/2015 16:29:49.

It shows quite unusual properties and behaviors compared to molecular colloids, whose dispersed phase consists of small molecules or molecular complexes. This paper describes the initial results of our study on the first single-nanodiamond particles mono-dispersed in water.

2. The colloid chemistry of nanodiamonds: state of the art

The colloid chemistry of the carbon nanomaterials and, in particular, of dispersed diamonds has a long history. The present study was undertaken to better understand the properties of the aqueous dispersion of 3 nm-sized positively charged nanodiamond species. First of all, the interaction with various ions and stability towards the coagulation were to be examined and discussed.

Similar systems with somewhat larger particles[11,12] have been described, whereas Raman spectra of the hydrosol under study were reported recently.[13] Using Raman photon confinement, the core diamond size was estimated to be 2 nm.[14]

Both positively and negatively charged ND species have been comparatively studied in water[4,5,15,16] and dimethyl sulfoxide.[17,18] The expressed dependence of the electrokinetic potential (zeta potential, ζ) on pH[4,15,16,19–23] and on the addition of inorganic electrolytes[22–25] has been reported as well as the size dependence on pH.[12,19,26] These observations have been discussed in terms of ion adsorption, interfacial acid–base reactions, and screening of interfacial electrical charges. Besides, the adsorption of a cationic fluorescent dye propidium iodide both on positively and negatively charged NDs has been studied in detail.[21,27]

Normally, the colloidal stability of entire, *i.e.*, stabilizer-free hydrosol is caused by the interfacial charges causing the formation of a protective double electrical layer. In the case of ND samples, however, the biographies of the surfaces are sometimes a matter of commercial secrecy. But even if the procedures of hard oxidation pre-treatment and the so-called de-agglutination procedure are transparent, and the properties are reproducible well enough, the completeness of the interface chemistries still allows considering the ND hydrosols as an (to some degree) ill-defined colloid system.

Theoretical consideration of the surface properties of ''bare'' ND primary particles[28–30] revealed the existence of [100] facets with positive electrical potential, whereas the graphitic [111] surfaces possess the negative potential. This finding rationalized the mechanism of spontaneous aggregation of the species into secondary ones.[28,29] It should be mentioned, however, that the ND colloids as a rule exhibit substantial values of zeta-potential. The latter cannot be caused by charge distribution within neutral species only.

The origin of the interfacial charge should be ascribed to the surface functional groups, which inevitably appear in processing the detonation soot to the final highly dispersed system. Such a ''forced modification'' generates a wide variety of ethers, lactones, pyrones, acid anhydrides, carboxylic and amino groups, amides, *etc.* Hence, it is important to identify these interfacial groups for any ND sample, taking into account that different procedures for processing the detonation soot are used nowadays.

Vibrational spectroscopy is the most often used tool to characterize the surface functional groups. A detailed consideration of the IR spectra of detonation ND has been proposed by Jiang and Xu.[31,32] From these and previous publications it may be concluded that most typical are the bands with wave numbers ≥ 3400 cm^{-1} (ν_{OH} bonded, ν_{OH} of water and ternary alcohol, ν_{NH} bonded), 2961–2887 cm^{-1} (ν_{CH}), 1783–1755 cm^{-1} ($\nu_{C=O}$ of ketones, lactams, esters and carboxyl groups), 1698–1587 cm^{-1} (δ_{OH} of water, $\nu_{C=O}$ of amides), 1480 (δ_{CH}), 1395–1254 cm^{-1} (δ_{CH}, ν_{CN}, $\nu_{C=O}$ ester, epoxy, δ_{CNH}), 1194–959 cm^{-1} (δ_{CCC}, δ_{OH}, δ_{COC}), and ≈ 550 cm^{-1} (δ_{CCC}, δ_{NCO}). The adsorption of water on both Lewis acid and base sites was shown to take place soon after the pellets are exposed to air.[33]

Mironov *et al.*[34] examined five different ND samples and ascribed the peaks of 3450–3430 cm^{-1} to ν_{OH}, 1790–1730 cm^{-1} to $\nu_{C=O}$ of carbonyl and carboxyl groups, and 2960–2880 cm^{-1} to C–H stretching in alkane hydrocarbon groups. The broad ranges of absorption at 1640–1620 and 1400–1300 cm^{-1} are superpositions of various bands with δ_{OH} of adsorbed water in the first case and δ_{CH} in the second. These authors also revealed vibrations of *O*-nitroso and nitro groups.[34] Based on different data, Kulakova[35] also revealed the $\nu_{C=O}$ bands (1790–1730 cm^{-1}), and ν_{OH} and δ_{OH} vibrations (3400 and 1640 cm^{-1}, respectively), whereas absorptions within the range of 1140–1100 cm^{-1} should be attributed to the ethers (C–O–C), NO_2, OH, COOH, and SO_3H groups. The existence of amido, amino, and cyano groups is also probable.[35] Xu *et al.*[36] attributed the 2930 and 2850 cm^{-1} bands to the asymmetrical and symmetrical stretching of C–H and 1765 cm^{-1} to C=O vibrations. Whereas the bands 3434 and 3429 cm^{-1} and 1629 cm^{-1} in the IR spectrum have been ascribed by Xu *et al.* to ν_{OH} and δ_{OH}, respectively, the authors also suppose the stretching and deformation N–H vibrations of amino groups at the corresponding wave numbers.[36] Similar conclusions for 3432 cm^{-1} have been made by Shenderova *et al.* for NH_2, =NH, and >NH groups and 1632 cm^{-1} to NH_2 and >C=C< groups, along with the attribution of 3573 cm^{-1} to OH (free), 2960–2858 cm^{-1} to methyl and methylene, 1799 and 1725 cm^{-1} to anhydride, 1120 cm^{-1} to C–OH, adsorbed CO, and CO_2, *etc.*[37] Desai *et al.*[23] also attribute the band 1637 cm^{-1} both to O–H and N–H bend vibrations; 2970–2856 cm^{-1} and 1382 cm^{-1} have been assigned, respectively to C–H stretch and bend vibrations, 3405 cm^{-1} to O–H (stretch), and 1122 cm^{-1} to C–O–C vibrations.[23] Mochalin *et al.*[38] attributed the band 1640 cm^{-1} in the Raman spectrum of ND to the superposition of graphitic C=C vibrations, O–H bending, and C=O stretch vibrations.

Generally speaking, it is not surprising that the detonation ND always contains around 2% of nitrogen. Therefore, besides the existence of the nitrogen defects of the diamond lattice which manifest themselves through photoluminescence, some authors assume the presence of nitrogen-containing groups on the surface.[5,16,23,31,32,34–37]

However, the N–H vibrations have frequencies close to the O–H vibrations. Therefore, the bands of nitrogen-containing

Published on 27 May 2015. Downloaded by University of California - San Diego on 02/06/2015 16:29:49.

groups overlap with those of O–H groups and may be somewhat hidden in the IR spectra. Some authors ascribe the vibration bands without taking into consideration the amino, amido, and nitro groups.[20,39–43] So, Krüger *et al.*[40] reported for different ND samples the bands around 3430 cm^{-1} (broad and intense) and 1630 cm^{-1} as stretching and deformation vibrations of associated OH groups, 1781–1707 cm^{-1} as $\nu_{C=O}$ of ketones, 2954–2851 cm^{-1} and 1460, and 1459 cm^{-1} (ν_{CH} and δ_{CH} vibrations for carbon atoms in the sp^3 state), 1416–1361 cm^{-1} and 1128, and 1114 cm^{-1} as δ_{COH} and ν_{C-O} of alcohols.

The FTIR data reported in some recent papers[4,16,20,41–44] may be summarized as follows. The region 3600–3200 cm^{-1} corresponds to ν_{OH} of alcohols, carboxylic groups, and adsorbed water (with the maximum at 3420 cm^{-1}); the weak band at 3690 cm^{-1} corresponds to the un-associated OH groups. The bands within the range of 2970–2856 cm^{-1} belong to the stretching of C–H groups, whereas the bands 2370 and 2086 cm^{-1} have been attributed to the CO_2 molecules adsorbed on the pellets and to ketenes, respectively. Stretching vibrations observed from 1865 to 1700 cm^{-1} give evidence for the presence of lactones, COOH groups, esters, and ketones. The absorptions at 1620–1630 cm^{-1} and some neighboring ones have been ascribed to δ_{OH} of water and in some cases also to the C=C and C=O groups, and the bands at 1384 and 1394 cm^{-1} to δ_{OH} of the carboxyl group and δ_{CH}, respectively. The band at 1456 cm^{-1} was attributed to the C=C vibrations,[43] whereas earlier it has been ascribed to δ_{CH}.[40] Absorption at 1370–1100 cm^{-1} corresponds to ethers, lactones, acid anhydrides, and epoxy groups. Also, the bending vibrations of the carboxylate groups C–O^- at 1370–1320 are reported.[42]

Finally, a broad absorption band peaks at around 1130 cm^{-1} caused by N defects in nitrogen-rich diamonds.[45]

Note that the above results refer as a rule to ND samples from different sources. The origin of the ND samples and subsequent procedures such as heating and hydrogen treatment influence the FTIR spectrum which reflects the alterations of the surface groups, *e.g.*, the mechanochemical treatment decreases the comparative intensity of carboxyl against amino groups.[30] The bands of oxygen-containing groups decrease and those of CH_2 groups (2920–2875 cm^{-1}) increase in the hydrogen-treated sample as compared with the untreated one.[15] Similar results of hydrogenation, as well as results on treatment in ammonia and chlorine, were reported earlier.[46] Similar changes have been observed as a result of heating at 700 °C in a vacuum,[19] and in both cases the negative zeta-potential of NDs in water turned to a positive sign. Recently Petit *et al.* demonstrated that heating at 750 °C leads to the loss of the COOH groups.[4] Oxidation with nitric + sulfuric acid under ultrasound[23] resulted in the appearance of a significant shoulder at 1728 cm^{-1}, in accordance with the carboxylation concept.[23] The colloidal behavior in water, however, was practically unaffected by such a procedure.[23] After modification of ND by amines, the N–H vibrations have been found at 1650 to 1450 cm^{-1}.[47] Another kind of aminated ND was studied in detail by Mochalin *et al.*[48] An intense band at 1665 cm^{-1} was ascribed to the vibrations of the secondary amide. The latter appears as a result of modifying the COOH-bearing ND by ethylenediamine; the strong peak of C=O stretch (1762 cm^{-1}) observed both for modified and non-modified ND should be attributed to the residual non-amide carbonyl groups.[48]

Evidently, the composition and hence the charge of the interfacial regions of ND primary particles govern the formation of the secondary colloidal species. As many properties are shown to be critically dependent on the ND size, centrifugation including ultracentrifugation[42,44,49] was used in order to fractionate the polydispersed colloidal system. As a result, even 3 nm-sized particles have been resolved from the starting sample.[42] On the other hand, the larger aggregates of primary 4–5 nm ND particles are found to be porous by using the BET adsorption and other methods;[24,49] some indications of the fractal structure have also been reported.[18,22] The viscosity of the ND hydrosols decreases along with dilution,[26] whereas the concentrated 10–12 wt/vol% system is actually a hydrogel. The addition of electrolytes finally results in coagulation,[23] whereas association of the positively charged ND species with the negative SiO_2 nanoparticles[16] should be considered as an example of mutual coagulation and also as adagulation, *i.e.*, coagulation through adherence of colloidal particles to solid surfaces of larger size. All these phenomena are of importance for using the ND hydrosols in various fields, especially in biomedicine, because of the presence of electrolytes in biological fluids.

The above-mentioned properties depend on the origin of the ND samples, but some principal features are of universal character. The unique small size and other peculiar properties of the ND particles chosen for the present study give the opportunity to re-examine the previously developed concepts and consider the systems of such a kind from a somewhat different angle of view.

3. Experimental

3.1 Preparation of the ND hydrosol

Primary particles of dispersed detonation nanodiamonds were provided by NanoCarbon Research Institute, where commercial crude grey powder of detonation nanodiamonds (manufactured by FMD Nano Tech Co., Guangzhou, China) was disintegrated in portions in a 150 mL attrition mill (constructed by Kotobuki Industries Co., Tokyo) using 30 μm zirconia beads in distilled water. Milling conditions have been locally optimized by applying Taguchi's Method of quality engineering[50] and will be disclosed shortly elsewhere. The product of bead milling is a black but translucent and smooth colloidal solution with 4 to 5 wt/vol% concentration of the primary particle of detonation nanodiamond (PPDND) having a typical average diameter of 3.0 ± 0.5 nm as determined using dynamic light scattering (DLS), from the size distribution by the particle number. This colloidal solution was used in this work virtually as is except for centrifugal separation at 5000 rpm for one hour. As an inevitable consequence of attrition milling, the product is contaminated with 0.4 wt% of zirconia, which has been so far difficult to remove.[51]

Published on 27 May 2015. Downloaded by University of California - San Diego on 02/06/2015 16:29:49.

3.2 Materials

Sodium chloride, perchlorate, and sulfate, barium and calcium chlorides, potassium iodide, ferri- and ferrocyanides, silver nitrate, ferrous sulfate, and hydrochloric acid were of reagent grade, sulfuric and nitric acids were of analytical grade, the aqueous solution of sodium hydroxide was prepared from saturated stock alkali solution using CO_2-free water and kept protected from the atmosphere. Cetyltrimethylammonium bromide (99%), cetyldimethylammonium propanesulfonate (>99%), and sodium *n*-dodecylsulfate (99%) were purchased from Sigma, sodium *n*-tetradecyl- and *n*-hexadecylsulfates were kindly donated by Professor Sergey N. Shtykov (Saratov State University, Russia), and high purity sodium *n*-octylsulfonate was put to our disposal by Dr Artem Yu. Kulikov from Analytical Chemistry Department (Kharkov V. N. Karazin National University). The dyes bromophenol blue, bromocresol green, bromocresol purple, methyl orange, fluorescein, sulfonefluorescein, and rose Bengal B were samples from the collection of the Department of Physical Chemistry (Kharkov V. N. Karazin National University), used and characterized in our previous studies; 5′-aminofluorescein was purchased from Sigma-Aldrich. Pseudoisocyanine iodide and the standard solvatochromic betaine dye 4-(2,4,6-triphenylpyridinium-1-yl)-2,6-diphenylphenolate (*ca.* $2H_2O$) were the gifts of Dr T. Shakhverdov and Professor C. Reichardt, respectively. Double-distilled water was used in all the procedures.

3.3 Apparatus

Electrical conductance measurements were carried out using platinized platin electrodes in molybdenum-glass cells using a Precision LCR Meter GW Instek LCR-817 apparatus operating at a frequency of 1 kHz. The cells were calibrated using 12 standard aqueous solutions of potassium chloride, within a concentration range of 1×10^{-4} to 0.01 M.‡ All the measurements were carried out at 25.00 ± 0.05 °C. The pH determinations were performed by using an R 37-01 potentiometer and a pH-121 pH-meter with an ESL-43-07 glass electrode in a cell with the liquid junction (4.00 M KCl). An Ag|AgCl electrode was used as a reference. The cell with the glass electrode was calibrated with standard buffers (pH 9.18, 6.86, 4.01 and 1.68 at 25 °C). The content of NO_3^- and Cl^- ions was determined for the 0.999 wt/vol% ND hydrosol. The NO_3-selective electrode ELIS-121NO_3 (Russia) was soaked for 24 h in 0.1 M KNO_3 aqueous solution and kept for two weeks in 0.001 M KNO_3. For 2 h before use, the electrode was placed in pure water. For calibration, 1.16×10^{-5} M, 1.16×10^{-4} M, 1.16×10^{-3} M, and 1.16×10^{-2} M KNO_3 solutions were used at 25 °C. An Ag|AgCl electrode was used as a reference electrode. For the liquid junction, KCl in agar–agar was used. The e.m.f. values were measured with the uncertainty of 0.1 mV, and the slope was 46.06 mV per pNO_3 (R^2 = 0.9986). The Cl-selective electrodes ELIS-131Cl (Russia) and Orion Research, Model 93-17 were soaked for 24 h in 0.5 M KCl solution and kept for a week in 0.001 M KCl. Before use, the electrode was placed in pure water. The 1.00×10^{-5} M, 5.00×10^{-5} M, 5.00×10^{-4} M, 5.00×10^{-3} M, 5.00×10^{-2} M, and 5.00×10^{-1} M KCl solutions were used for cell calibration at 25 °C. An Ag|AgCl electrode was used as a reference electrode, with KNO_3 in the agar–agar liquid junction. The calibration slopes for the electrodes were 51.95 mV per pCl (R^2 = 0.9995) and 46.00 mV per pCl (R^2 = 0.9939), respectively. For the viscosity measurements, the apparatus VPZh-2 (Russia) with a capillary diameter of 0.56 mm was used at 25.0 ± 0.2 °C. The uncertainty of time measurements was ±0.1 s. The particle size distribution and zeta-potentials were determined *via* DLS using a Zetasizer Nano ZS Malvern Instrument apparatus at 25 °C, at a scattering angle of 173° in the National University of Food Technologies, Kiev, Ukraine. Some preliminary experiments were made in the Laboratory of Professor Paavo Kinnunen, Department of Biomedical Engineering and Computational Science, Aalto University, Espoo, Finland. For quantitative measurements, the clear disposable zeta cell was used; some prior estimates were made utilizing a zeta dip cell. The particle size distribution was measured by the static light scattering (SLS) method using a laser diffraction particle size analyzer SALD-7100 Shimadzu instrument. These determinations were made by E. A. Korosteleva in the Laboratory of Pharmstandart-Biolik, Kharkov, Ukraine. For the electron microscopy studies, a Selmi TEM-125K microscope was used. The procedure is as follows. In a vacuum vessel VUP-5M, a 10–20 nm carbon film was deposited from the Volta arc on freshly cleaved KCl monocrystals at the pressure of residual gases of around 10^{-5} Torr. After floating off in distilled water, the carbon films were picked up on copper electron-microscopy grids. The portions of the examined solutions were deposited on the films and studied after drying in the bright-field and diffraction modes of the TEM at an accelerating voltage of 100 kV. The images were registered using the CCD camera or photographic plates. For detection of the chemical elements in the sample by energy-dispersive X-ray spectroscopy (EDX), a droplet of concentrated ND solution was placed on a silicon wafer and after drying EDX analysis was performed on a SEM JSM-840 fitted with a Selmi EDS-1 spectrometer. The spectrometer is capable of registering elements with $Z > 5$. Absorption spectra were recorded using Hitachi U-2000 and SF-46 spectrophotometers against solvent blanks; the cuvettes with optical path length l = 0.1, 1.0, and 5.0 cm were used. The IR spectra were recorded by Dr D. Yu. Filatov with ALPHA's Platinum ATR and in KBr pellets using a FTIR spectrometer SPECTRUM ONE (PerkinElmer) in the range of 400–4000 cm^{-1} by Dr D. S. Sofronov, Division of Functional Materials Chemistry, Institute for Single Crystals, National Academy of Science of Ukraine. Fluorescence spectra were recorded using a Hitachi 850 apparatus. The Fe content was determined using an atomic absorption spectrophotometer, Selmi, Ukraine.

3.4 Procedure

The coagulation of the ND hydrosols has been studied at 25 °C using two somewhat different procedures. (i) The main values of the critical concentrations of coagulation (or coagulation points, or coagulation thresholds), CCC, by the electrolytes have been determined using the procedure of spectrophotometric titration, accompanied by slight stirring. In this case,

‡ Hereafter, 1 M = 1 mol × L^{-1}.

This journal is © the Owner Societies 2015

Published on 27 May 2015. Downloaded by University of California - San Diego on 02/06/2015 16:29:49.

both the (slight, not more than 1.5-fold) dilution of the initial solution by the electrolyte and alteration of the blank (electrolyte-free) solvent as a result of dilution with corresponding amounts of pure water (including the deviations from the Bouguer–Lambert–Beer law) were taken into account. (ii) The absorption spectra of the sets of solutions with constant ND content and varying electrolyte concentrations have been recorded immediately and within a period of time. In both cases, the criterion of the rapid coagulation was the distinct increase in the absorbance (mainly at 525 nm) caused by the turbidity of the systems under study. The solutions have been prepared and titrated in such a manner that allowed avoiding the high local concentration of the electrolytes. Namely, the initial concentrations were diluted enough, taking into account the CCC value of the given electrolyte determined in preliminary experiments.

The dye concentrations were around 1.0×10^{-5} M and in some cases even lower. All the spectra are presented after subtracting the adsorption of the ND solution; otherwise, the measurements have been made against the solvent blank. During the determination of the apparent ionization constants of the indicator dyes, the spectral measurements were made in diluted (1.0×10^{-4} to 0.001 M) HCl solutions.

4. Results and discussion

4.1 Characterization of the samples

In this study, two initial solutions with almost identical properties have been used. The principal numerical parameters of these aqueous hydrosols are compiled in Table 1. Hereafter, all the ND concentrations will be expressed in wt/vol%.

The origin of the positive charge of colloidal species will be discussed in the following sections of this paper. The size distribution of the dispersed system appeared to be strongly concentration-dependent, as exemplified in Fig. 1. Such a phenomenon should be evidently attributed to the formation of secondary aggregates along with dilution (see below).

The electron diffraction patterns reveal a diamond lattice of the sample. The lattice parameter was measured to be 0.375 ± 0.002 nm, and it coincides with the tabulated values for diamond within the error. The size of the coherence area, estimated in accordance with the Selyakov–Scherrer equation [eqn (1)],[52,53] is ≈3–4 nm.

$$d = \frac{\lambda}{\beta \cos\theta} \quad (1)$$

Here β stands for the intrinsic line broadening, θ is the scattering angle, and λ is the wavelength. Specimen tilt does not change the relative intensity of the diffraction lines which, in conjunction with the small size of the coherence area reveals a nano-size structure in the sample. Together with the non-diamond surface structures, the size of the colloidal species is 2.8 ± 0.6 nm as found *via* DLS, while the diamond core size is 2 nm, as mentioned above. The above-mentioned non-diamond portions may be probably of graphitic character,[12,28,29] or even a kind of graphene patch. Because the disaggregation of the agglutinates has been made without any chemicals, the interfacial concentration of the functional groups may be relatively low. The numerical concentration of the initial sol was calculated expecting a doubly truncated octahedron shape for the primary particles as the most probable[29] and using the density value of 3.17 g cm^{-3}.

Table 1 Characterization of the initial concentrated ND hydrosols

Parameter	Sample 1[a]	Sample 2[b]
Concentration/(wt/vol%)	3.81	5.0
Particle size[c]/nm	3.0 ± 0.5[d]	2.8 ± 0.6[d]
Numerical concentration, L^{-1}	8.5×10^{20}	11×10^{20}
pH, 25 °C	4.75	5.00
ζ/mV for 1.0 wt/vol%	+58.1[e]	+56.7[e]
Viscosity/mPa s, 25 °C	2.45	2.23
Specific conductance/S cm^{-1} for 1.0 wt/vol%	n.m.	7.18×10^{-5}
Cl^-/M	n.m.	2.75×10^{-3}
NO_3^-/M	n.m.	2.5×10^{-5}
N content in the solid/wt%	2.0	2.0
ZrO_2 content in the solid/wt%	0.4	0.4
Fe/ppm	n.m.	24[f]

[a] Sample 1 was studied from August 9, 2013 to December 12, 2013. [b] The sample was studied from December 13, 2013. [c] The mean size (diameter) of the smaller-size fraction. [d] The size was determined at NanoCarbon Research Institute, Japan; in National University of Food Technologies, Ukraine, the particle size for the 5% hydrosol was found to be 2.71 ± 0.35 nm (an average of 20 measurements). [e] In National University of Food Technologies, Ukraine, the ζ = +50.1 ± 2.7 mV value (an average of 9 measurements) was determined for the concentration of 2.5 wt/vol%. [f] Determined by atomic absorption.

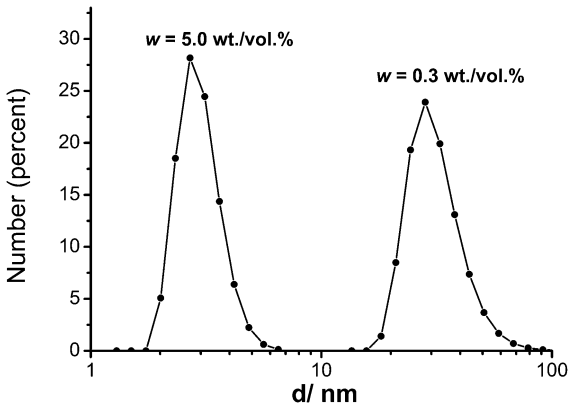

Fig. 1 Size distribution of the stock colloidal ND solution, 5.0% and diluted 0.3% ND solution.

The IR spectra of the solid samples (Fig. 2) have been obtained after drying either the 0.603% hydrosol or the system coagulated by sodium hydroxide and then centrifugated.

The main bands resemble those reported by Korobov *et al.* for the NanoAmando sample.[42] Along with the stretching vibrations of the bound OH and maybe NH groups (3428–3421 cm^{-1}), some small sign of free ν_{OH} may be observed at 3747–3687 cm^{-1}. The C–H stretching modes at 2923–2853 cm^{-1} are also present in the spectra, whereas the band with the maximum at 1623 cm^{-1} should be attributed to δ_{OH} vibrations; the δ_{NH}, C=C (graphitic), and $\nu_{C=O}$ (amides) vibrations also cannot be excluded in the same region. The C=O stretching of lactones and COOH groups (1715 cm^{-1}) is less expressed.

Published on 27 May 2015. Downloaded by University of California - San Diego on 02/06/2015 16:29:49.

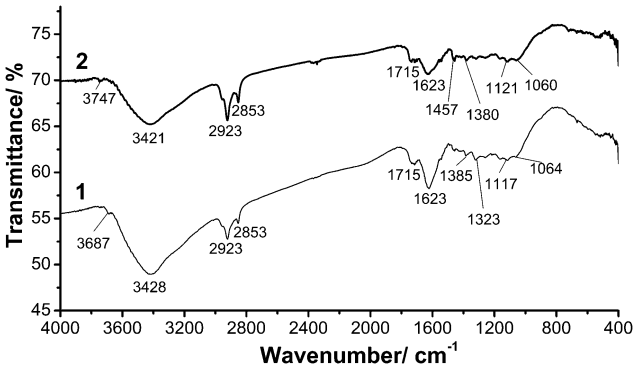

Fig. 2 The IR spectra of KBr pellets of solid ND obtained from the 0.603% hydrosol: the sample was obtained by drying the colloidal system (1) and by drying the deposit after coagulating by 6.7×10^{-4} M NaOH using further centrifugation (2).

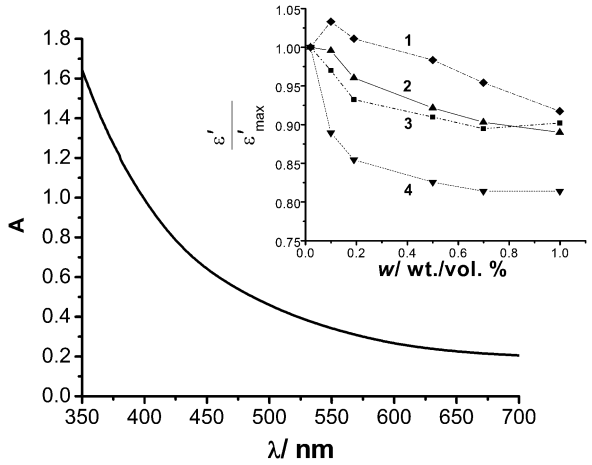

Fig. 3 Absorption spectrum of the 0.19% ND hydrosol. Inset: the verification of the Bouguer–Lambert–Beer law, $\varepsilon'/\varepsilon'_{max}$ is the normalized absorptivity; $\varepsilon' = A/wl$; wavelengths per nm: 400 (1), 525 (2), 600 (3), and 650 (4).

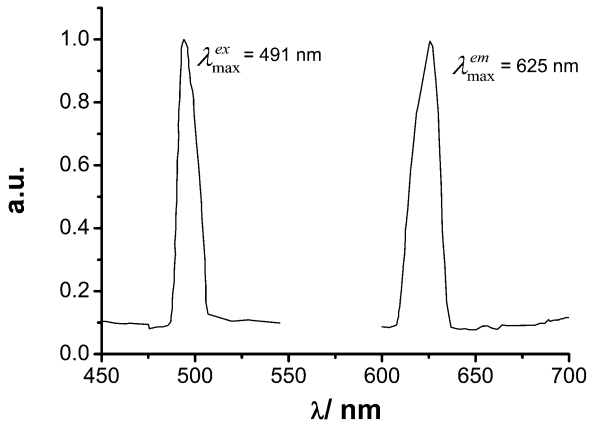

Fig. 4 The fluorescence excitation and emission spectra of the 0.19% ND hydrosol.

The band at 1457 cm^{-1} may belong to δ_{CH} (for the carbon atom in the sp^3 state) and vibrations of amides and C=C bonds. The absorption within 1385 and 1060 cm^{-1} can be ascribed to C–O–C ethers and other oxygen-containing groups, as well as to δ_{CH}, δ_{CH}, δ_{CNH}, and ν_{CN} and to nitrogen defects in the crystal structure (see the Introduction section). The IR spectra of the sample on the diamond plate are given in the ESI.†

In the solid phase, the EDX spectra revealed, besides carbon, 0.28 Cl and 0.28 Zr (wt%, ±0.14 wt%); no sulfur was observed above 0.02 wt%. The analysis of the liquid phase was also necessary in order to have a complete picture of the system, first all of the anions present in water, which compensate the positive charge of the colloidal species.

The qualitative analysis of the liquid phase was made after coagulation of the colloidal system by diluted NaOH (for details see below), separation of the deposit, and neutralization of the liquid with either H_2SO_4 (for the determination of nitrates) or HNO_3 (for the determination of other anions). The reaction with $FeSO_4$ and conc. H_2SO_4 revealed the presence of nitrates: a brown ring indicates the formation of the $FeNO^{2+}$ ion.[54] On the other hand, the reaction with $AgNO_3$ showed the presence of chlorides, whereas that with $BaCl_2$ gave no evidence for sulfates. The quantitative determination of the chloride and nitrate concentrations was made directly in the sol using the corresponding ion-selective electrodes. In 1.00% ND hydrosol, the Cl^- content was $(5.5 \pm 1.3) \times 10^{-4}$ M. This chlorine content is in line with the rough estimate by EDX (see above). The nitrate content appeared to be small; *e.g.*, in 1.00% ND solution, the conc. NO_3^- content of $(5 \pm 1) \times 10^{-6}$ M was found.

4.2 Optical properties of the ND hydrosol

The light absorption increases gradually in the range of wavelengths from 700 to 350 nm, and the solutions do not strictly obey the Bouguer–Lambert–Beer law (Fig. 3). The absorption coefficient, $\varepsilon' = A/wl$, increases along with the dilution. It should be noted that, regardless of the contribution of light scattering and the balance between consumptive and conservative light absorption, we used the absorbance measurements just as a tool for monitoring the changes in the state of solutions. We believe that the absorbance refers first of all to the turbidity increase caused by the coagulation.

The fluorescence maximum is at 625 nm (Fig. 4), while the emission excitation maximum is at 491 nm, just near the line of the argon-ion laser (488 nm). The probable origins of the emission are the crystal lattice defects of N–V type. After coagulation by NaCl and six-fold dilution, the same bands are registered. These findings may be of interest for the utilization of ND in biomedical research.

4.3 Surface charge of the colloidal species

The zeta-potential of the species is substantially positive (Table 1) and varies along with dilution and changes more or less upon adding electrolytes or aging. The specific conductance of diluted ND solutions at 25 °C was determined (the data are presented in the ESI†). The value for the 1.00% ND solution is close to 5.49×10^{-4} M KCl: 6.87×10^{-5} and 7.80×10^{-5} S cm^{-1}, respectively. Hence, judging by this criterion the initial 5.00% hydrosol corresponds to 2.4×10^{-3} M KCl. This approximately

Published on 27 May 2015. Downloaded by University of California - San Diego on 02/06/2015 16:29:49.

agrees with the above-estimated concentration of Cl^- ions in the same ND solution.

Anionic dyes are readily adsorbed on the colloidal particles, thus confirming the positive charge of the ND/water interface (Fig. 5). In these experiments, the ND concentration was as a rule 0.048%. The observed 6 to 23 nm bathochromic shifts of the bands of the double charged anions of bromophenol blue, bromocresol green, bromocresol purple, fluorescein, sulfonefluorescein, aminofluorescein, and rose Bengal B (see ESI†) may be taken as a strong support for the positive interfacial charge of the colloidal species, because the same shifts are typical for these dyes in the presence of cationic surfactant micelles and aggregates of cationic dendrimers and calixarenes.[55,56]

By contrast, the absorption band of the cationic dye pseudoisocyanine displays no shift in the presence of the ND particles; only small alteration of intensity is registered. These results support the significant role of the ND charge for adsorption of organic species such as fluorescent ions[21,27] and daunorubicin.[39] It should be noted that, after coagulation of the ND hydrosol by NaCl, the position of the absorption bands of bromophenol blue and pseudoisocyanine is the same as in the sol without addition of the salt.

4.4 Colloidal stability and coagulation by inorganic electrolytes

The main working ND concentration in our studies with different electrolytes was 0.19%. In some experiments, the solutions of either higher or lower concentrations were used. The first results have been obtained using sample 1 (Table 1), the volume of which was limited. Therefore, the titration procedure has been used. The UV-visible absorption was used to monitor the coagulation process. The turbidity-caused increase in the absorption by 15% was chosen as a criterion of the rapid coagulation. The titration procedure is typified in Fig. 6. The titration curves were corrected both for the electrolyte concentration and the ND absorption by taking into account the dilution during the titration procedure.

As the concept of the threshold of rapid coagulation, or coagulation points, or critical coagulation concentration, CCC, is somewhat conditional and sometimes even subjective, we tried to standardize the procedure with much larger amounts of sample 2. In Fig. 7 and 8, the dependencies of the absorbance *vs.* time are exemplified. Both procedures carried out with NaCl for 0.19% hydrosols obtained by the dilution of sample 1 and sample 2 resulted in coinciding CCC values. The comparison of the two procedures was carried out also for NaOH and some other electrolytes.

The coincidence of the two methods of CCC determination is additionally proved using the DLS measurements. In Fig. 9, the distinct increase in the size of aggregates occurs on going from 2.0 to 3.0 mM NaCl, whereas the slight shift of curve (2) against curve (1) is probably caused by the 1.5-fold dilution of the initial ND sol. These results are in accord with the SLS measurements (see ESI†).

The DLS data for 0.13% and 0.024% ND with 1.1 mM NaOH, *i.e.*, well above the CCC, indicate particles of over 2 μm. The expressed increase of the size was reported for different ND samples at low and high pH values, *i.e.*, during coagulation *via* acid and alkali, respectively, by other authors.[12,26] Mochalin *et al.*[48] observed such an effect for colloidal particles of ND modified by amino groups on going from pH 2 to 6, whereas for COOH-bearing ND species, the effect was reverse and the decrease in the size of colloidal particles was observed, probably owing to the ionization of the functional groups, thus preventing coagulation.

The repeatability of the CCC values shown in Table 2 is satisfactory. These data are in line with the positive charge of the colloidal species. Indeed, the Schulze–Hardy rule predicts the sharp increase in the coagulation power of multi-charged well-hydrated inorganic anions in the case of "positive" sols. In fulfillment of this rule, the ratio of the reciprocal CCC values for the anions Cl^-, SO_4^{2-}, $Fe(CN)_6^{3-}$, and $Fe(CN)_6^{4-}$ is as follows: 1 : 16 : 200 : 583.

It is well known that for small colloidal particles, the coagulation threshold is often fuzzy.[57] However, for NaCl the rapid coagulation takes place certainly between 2.5 and 3.0 mM (Fig. 7 and 8).

The Derjaguin–Landau–Verwey–Overbeek (DLVO) theory in its classical version for highly charged surfaces of colloid

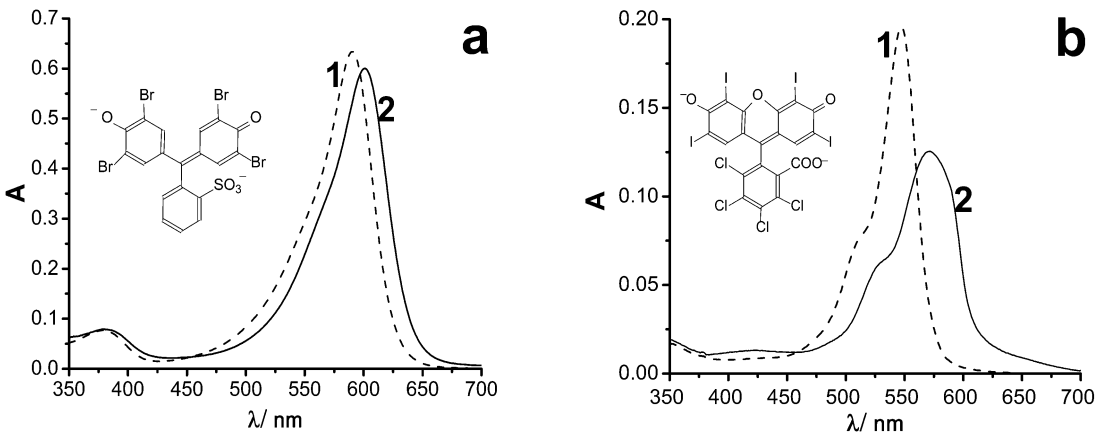

Fig. 5 Bromophenol blue (a) and rose Bengal B (b) in water (1) and in ND 0.048% solution (2).

Published on 27 May 2015. Downloaded by University of California - San Diego on 02/06/2015 16:29:49.

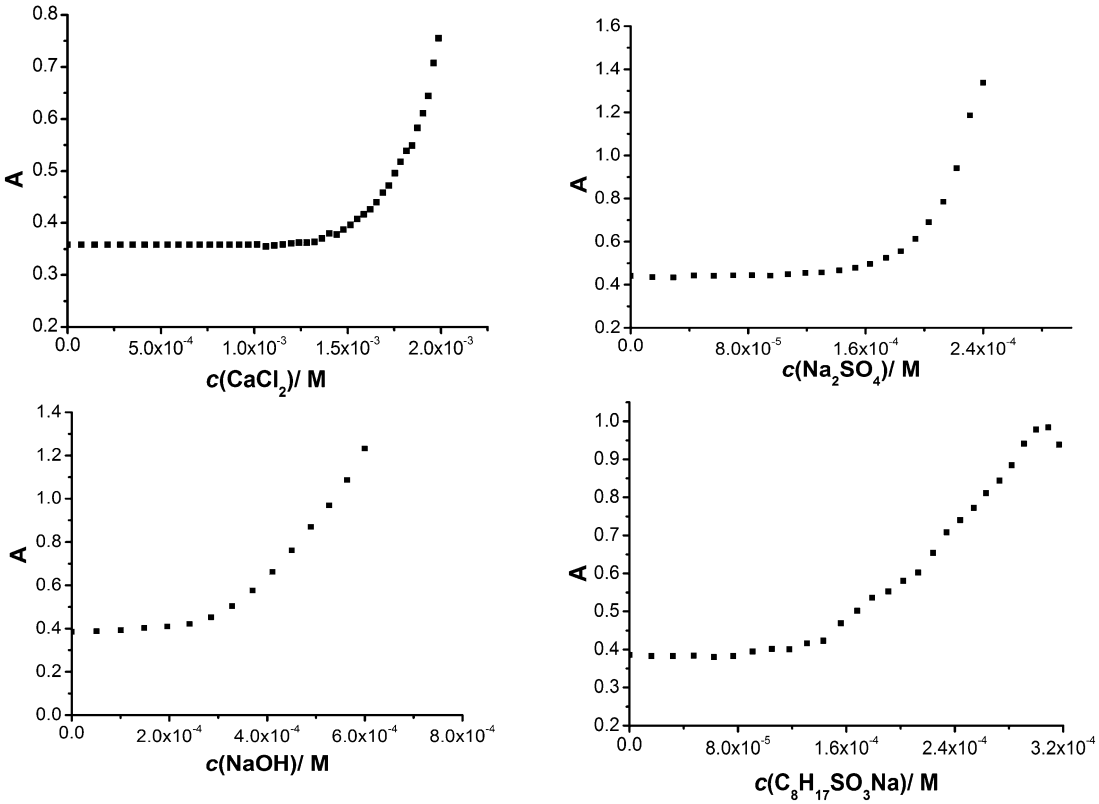

Fig. 6 Examples of CCC determination of the 0.19% ND hydrosol *via* titration with solutions of different electrolytes; the measurements have been made at λ = 525 nm.

species predicts the following dependence of CCC *vs.* counter-ion charge, z:

$$\mathrm{CCC} = \mathrm{const} \times z^{-n}, \qquad (2)$$

where n equals 6.[58–61] Lower n values, such as 2, 2.5, 3.5, or 4, also have been registered.[58–61] They should be explained either in terms of coagulation in the "distant minimum", *i.e.*, through the water layers, or by adsorption of counter ions and low surface charges, and also by taking into account the retardation of the molecular forces.[58,59] In our case, the average n value is in-between 4.0 and 4.8.

The Schulze–Hardy rule seems to be of universal character. For instance, it holds for a wide variety of organic and inorganic "negative" colloids[62] including different nano-carbons discovered during recent decades. So, for Na^+, Ca^{2+}, and La^{3+} the ratio of the reciprocal CCC values equals 1 : 185 : 740 and 1 : 21 : 1518 in the case of SWCN suspension[63] and C_{60} hydrosol,[64] respectively. Very recently, the last data were confirmed by the ratio of 1 : 27 : 1291 for fullerene suspensions.[65]

For the positively charged large-sized ND aggregates, Desai *et al.*[23] reported the CCC values of 8 to 10 mM for NaCl and 7 to 8 mM for $MgCl_2$. This also demonstrates the secondary role of the simili ion as compared to that of the counter ion.

Also, the single-charged anions are arranged with respect to their coagulation strength in tentative accordance with the lyotropic (Hofmeister) series, though with the inversion of iodide and perchlorate: $Cl^- < Br^- < ClO_4^- < I^-$. For perchlorate and iodide, the specific adsorption mechanism is probable, in addition to the screening of the interfacial charge of the ND aggregates. The surfactant cetyltrimethylammonium bromide acts just as a salt with the Br^- anion. The concentration of the latter ion under such experimental conditions is around the critical micelle concentration, *i.e.*, about 1 mM. The CCC = 1.6 mM value is even higher, probably owing to the adsorption of the cation on the ND species, thus increasing the colloid stability.

Note that both cationic $C_{16}H_{33}N(CH_3)_3^+Br^-$ and zwitter-ionic $C_{16}H_{33}N(CH_3)_2^+–(CH_2)_3SO_3^-$ amphiphiles display no special influence on the ND sol stability, whereas the *n*-dodecylsulfate ion, $C_{12}H_{25}OSO_3^-$, as well as other anionic surfactants exhibits strong coagulating influence. The latter is evidently caused by the electrostatic neutralization of the positive surface of the nanoparticles by the readily adsorbed amphiphilic anions; the hydrocarbon tails became (probably) directed towards the aqueous phase, thus increasing the hydrophobicity of the colloidal species.[66,67] Interestingly, as opposed to the cases of negatively charged C_{60} nanoparticle + cationic surfactant[64] and positively charged ND species + sodium oleate,[36] here the excess of the surfactant does not stabilize the ND colloid by the formation of "tail-to-tail" bilayers.

The titration curves in the case of surfactants and highly charged $Fe(CN)_6^{3-}$ and $Fe(CN)_6^{4-}$ ions are less distinct as compared with other data (see Fig. 6 and ESI†). This should be attributed to the prevailing adsorption mechanism.

 This journal is © the Owner Societies 2015

Published on 27 May 2015. Downloaded by University of California - San Diego on 02/06/2015 16:29:49.

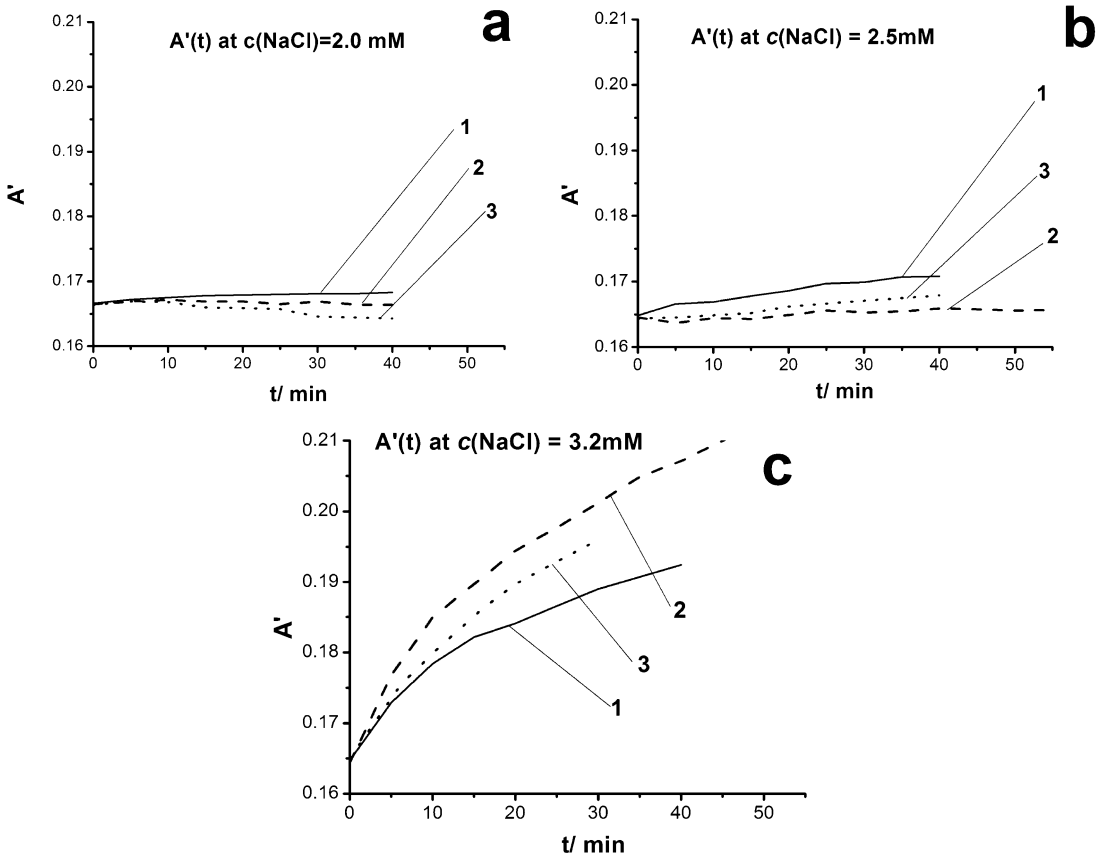

Fig. 7 The time dependencies of the absorption at NaCl concentrations of 2.0 mM (a), 2.5 mM (b), and 3.2 mM (c); the ND concentrations, %: 0.024 (1), 0.13 (2), and 0.67 (3). The conventional *A′* values were obtained by displacement of the starting point to that for 0.13%.

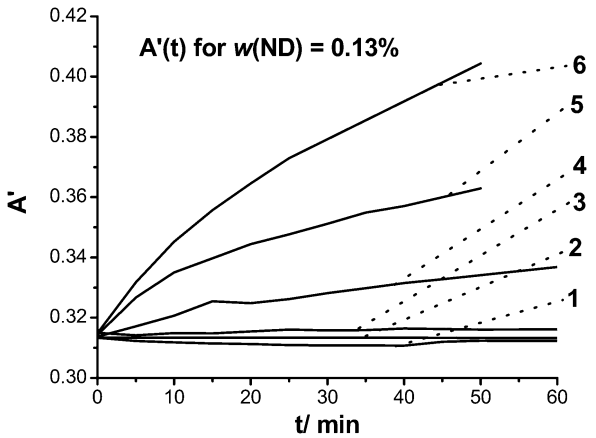

Fig. 8 The time dependence of the absorbance of 0.13% ND hydrosol at NaCl concentrations of 1.0 mM (1), 2.0 (2), 2.5 (3), 3.0 (4), 3.2 (5), and 3.5 mM (6).

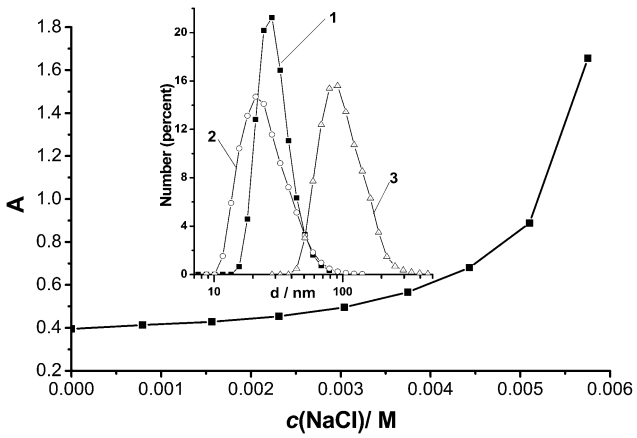

Fig. 9 The spectrophotometric titration curve of the ND hydrosol at the initial concentration of *w* = 0.19% by NaCl: absorbance at a wavelength of 525 nm *vs.* the NaCl concentration in the optical cell. The inset shows the DLS size distribution of the initial 0.19% ND solution (1) and 0.13% solutions with 2.0 mM (2) and 3.0 mM (3) NaCl.

Indeed, despite the high negative charge of the above inorganic anions the corresponding CCCs may be too low to critically condense the diffuse part of the double electrical layer. Therefore the adsorption and thus neutralization of the positive interfacial charges probably play a significant role. On the other hand, the number of $Fe(CN)_6^{3-}$ and $Fe(CN)_6^{4-}$ anions within the coagulation region is 3 to 9 times lower than that of primary 2.8 nm-sized ND species. Probably, the ''neutralization'' mechanism, *i.e.*, the adsorption of the anions and thus the decrease in the interfacial electrical potential cause the

Published on 27 May 2015. Downloaded by University of California - San Diego on 02/06/2015 16:29:49.

Table 2 The coagulation points, CCC/mM, of the 0.19% ND hydrosol

Electrolyte	CCC	z of the anion	CCC_{NaCl}:CCC
NaCl	2.8	−1	1.00
HCl	5.7	−1	0.49
$1/2CaCl_2$	2.4	−1	1.2
NaBr	2.5	−1	1.1
$C_{16}H_{33}N(CH_3)_3Br$	1.6	−1	1.75
$NaClO_4$	1.8	−1	1.6
KI	0.76	−1	3.7
NaOH	0.27	−1	10
$C_8H_{17}SO_3Na$	0.15	−1	19
$C_{12}H_{25}OSO_3Na$	0.039	−1	72
$C_{14}H_{29}OSO_3Na$	0.031	−1	90
$C_{16}H_{33}OSO_3Na$	0.041	−1	68
Na_2SO_4	0.17	−2	16
$K_3Fe(CN)_6$	0.014	−3	200
$K_4Fe(CN)_6$	0.0048	−4	583

coagulation in concert with the ''concentration'' mechanism, or condensing of the diffuse layer. Indeed, the significance of properly accounting specific adsorption for understanding the Schulze–Hardy rule has been again underlined recently by Lyklema.[68,69]

Another anion which acts specifically is the hydroxide. This most hydrophilic ion displays the most expressed coagulation influence among the single-charged inorganic anions.

4.5 The acidic nature of the surface charge

Such a behavior of the OH^- ion provides evidence for the acidic origin of the positive charge of ND species. In contrast to the abnormal effect of NaOH, the CCC value for HCl is somewhat elevated as compared with that of NaCl. The reason may be the additional protonation of some residual basic interfacial groups, thus increasing the surface charge, electrical potential, and thus the colloidal stability. In some experiments, we managed to confirm it by registering a small (about several mV) increase of ζ value. Interestingly, small HCl concentrations increase the size of the aggregates to a certain extent. Probably, the protonation of the residual basic groups favors the repulsion of the primary species in the secondary aggregates, without breaking them apart, resulting in ''swelling'' of the aggregates.

The observations were antipodal in the case of NaOH. For instance, for the 0.19% ND hydrosol, ζ = +43.3 ± 1.7 mV. After adding to 2 mL of the sol 1 mL of 0.009 M NaCl, the ζ value of +41.3 ± 1.5 mV was registered, while the same experiment with 0.003 M NaOH resulted in a ζ drop of up to +15.0 ± 0.6 mV. The procedure was repeated with 0.036% ND, and the values for the neat sol and those diluted with NaCl and NaOH were as follows: ζ = +62.2 ± 0.8, +33.2 ± 1.8, and +12.4 ± 0.3 mV, respectively. Hence, the effect of the alkali is caused first of all not by the screening of the surface charge, but by the acid–base reaction. (Interestingly, even at $C_8H_{17}SO_3^-$ concentration two times lower than CCC the ζ potential of the ND hydrosol remains practically unaffected.)

Fig. 10 demonstrates the irreversibility of the coagulation of the sol by the alkali. Indeed, after coagulation by NaCl

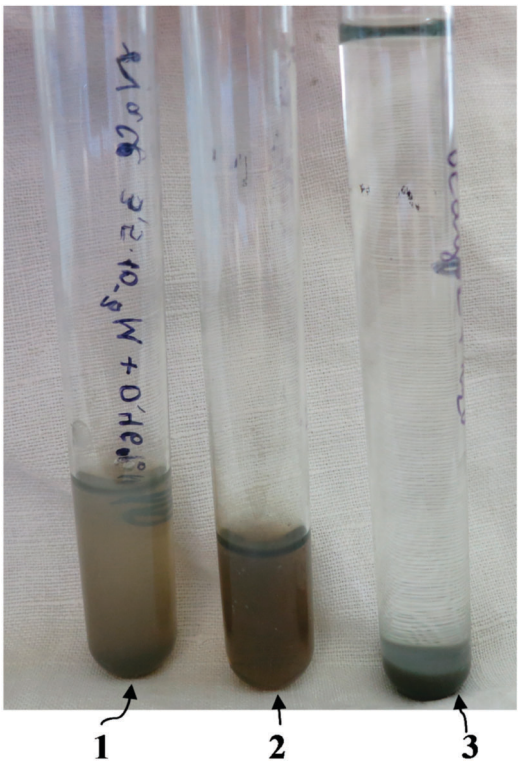

Fig. 10 The results of the peptization procedure: the 0.19% ND hydrosol, coagulated by NaCl (3.5×10^{-3} M) and then diluted by water (1); the initial hydrosol of the 0.19% ND (2); the same sol coagulated by NaOH (4.0×10^{-4} M) and diluted by an even larger portion of water (3). The samples (1) and (3) were shaken after dilution and left to remain 15 min before being photographed; after several days the picture remains unchanged.

around the CCC value, the colloidal system is easily restored just by slight dilution. This is typical for the case of coagulation caused by compression of the diffuse layer around the colloidal species: dilution restores the pre-threshold salt concentration. If the coagulation is accomplished by the alkali, the addition of a large amount of water displays no change in the deposited coagulate.

Instead of this dilution procedure, complete neutralization of the alkali by HCl does restore the hydrosol (see ESI†). Of course, the final electrolyte concentration, in fact NaCl, should not reach the corresponding CCC. (It should be noted, however, that if the ND hydrosol is stored for a day after coagulation by NaCl, dilution could not restore the colloid system even if the concentration of NaCl drops below 1 mM. Probably, the expulsion of water layers from the space between both primary and secondary ND particles takes place due to IICI or even, less likely, CICI attractions, see the Introduction section.)

This gives plane evidence for the occurrence of the acid–base neutralization of the interfacial positively charged groups by the HO^- ions, which is impossible to revert by dilution with water. These groups may be protonated alcohols or ethers, pyrones, ammonium groups or lyonium ions attached to some of the negatively charged [111] facets of the diamond exposed to

Published on 27 May 2015. Downloaded by University of California - San Diego on 02/06/2015 16:29:49.

the water phase.[12,15,16,25,36,70] Reasoning from the IR spectrum of our ND sample, we cannot exclude the presence of different functional groups, given below.

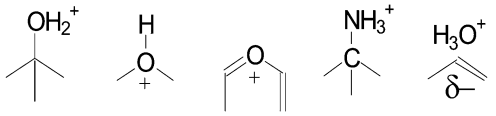

In the last case, the local positive interfacial potential of the [100] facets (not shown) may cause the positive zeta-potential of the ND species after protonation of the negative [111] graphitized facets (designated as $\delta-$).

However, if the protons are attached to the ND species from water only during the disintegration procedure, then the bulk liquid should be slightly alkalified, or, at least, possess a pH of around 6 due to carbon dioxide from the atmosphere. But this is not the case, and the pH value of the 5.0% hydrosol was always about 5. Hence, the admixture of acidic matter, probably HCl, in the initial commercial product is very probable.

Another argument represents the pH-metric titration of the hydrosol by NaOH solution. In Fig. 11, the most obvious example is shown; higher NaOH concentrations lead to rapid precipitation, whereas using lower ones leads to less expressed titration curves.

The equivalence point corresponds to 1.11 ± 0.27 mM NaOH, which means 2.5 ± 0.6 mM of the neutralized groups in the initial 5.0% sol, or 0.050 moles of groups per kg of the solid ND. (For the 3 nm ND particles, the interfacial concentration is equal to 4.8 groups per 100 nm^2.) Kulakova reported the much higher values for larger ND species of another origin.[35] Note that the Cl^- concentration in the 5.0% sol equals 2.8 ± 0.6 mM. Although the confidence intervals of these two average concentrations overlap, the second one is somewhat higher. If the positive charge of the colloidal species equals the total concentration of the anions in the bulk, and some amount of other (undetected) anions besides Cl^- and the trace amounts of NO_3^- cannot be excluded, some cationic groups may be considered as still not titrated by NaOH. Furthermore, a part of the alkali may be spent for the reaction with the neutral interfacial COOH groups, if they are really present. Last but not least: even after adding an excess of alkali, the ζ value drops sharply but remains positive within +(12–15) mV. Similar results were reported for solutions of some "positive" ND species of different origins, in some cases even at pH 11–12.[4,12,15,16,36] (But for some ND samples, re-charging resulting in $\zeta < 0$ was observed.[4,20,22,36]) This gives evidence for assuming the presence of some interfacial cationic centers of extremely low acidic strength, *e.g.* some metal ions originating from the detonation and oxidation stages. Although the solid ND contains the ZrO_2 admixture, this oxide is rather inert. Also, some cations may be hidden below the non-diamond surface structures, or even within the thin layer of disordered diamond.

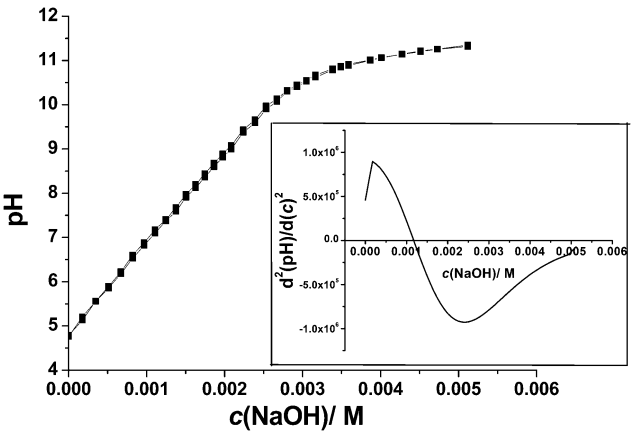

Fig. 11 The titration curve for 2.5% ND hydrosol with 0.00899 M NaOH solution; inset: the second derivative differential curve.

4.6 Estimation of the interfacial electrical potential of the ND species using the acid–base indicators

In order to achieve the comprehensive characterization of the system under study, an attempt was made to estimate the interfacial electrical potential of the colloidal species. If an acid–base indicator is located on the charged interface, the indices of the so-called apparent ionization constant may be determined by spectrophotometry:

$$pK_a^{app} = pH + \log\frac{[\text{acidic form}]}{[\text{basic form}]} \quad (3)$$

The pH value refers to the bulk phase and can be measured using the glass electrode in a cell with the liquid junction, while the concentration ratio of the equilibrated acid–base couple is available *via* the absorption spectra. Thus the obtained pK_a^{app} value is related to the interfacial potential or Stern layer potential, Ψ, through eqn (4):[71–73]

$$pK_a^{app} = pK_a^{i} - \frac{\Psi F}{2.303RT} \quad (4)$$

Here F is the Faraday constant, R is the gas constant, T is the absolute temperature, and K_a^i is the so-called intrinsic ionization constant. Then the Ψ value at 25 °C is:

$$\Psi/\text{mV} = 59.16\ (pK_a^{i} - pK_a^{app}) \quad (5)$$

The pH values are normally adjusted using buffer systems. In the case of the ND hydrosol, however, the addition of the buffer electrolytes results in coagulation. Fortunately, the coagulating action of diluted HCl solutions is not that strong (see above). Therefore, a set of indicator dyes should be used with the color transition in the pH range of 3–4. Within this narrow limit, the pK_a^{app} values are determinable, whereas the buffer capacity at lower HCl concentrations is insufficiently small. Another requirement consists of the availability of the spectra of the limiting acidic and basic forms under conditions which exclude the coagulation of the sol. The dyes chosen for this experiment were all of anionic type; their ionization occurs according to the following scheme:

$$HR^- \rightleftarrows R^{2-} + H^+ \quad (6)$$

The sulfonephthaleins bromophenol blue, bromocresol green, and bromocresol purple display the color transition

Published on 27 May 2015. Downloaded by University of California - San Diego on 02/06/2015 16:29:49.

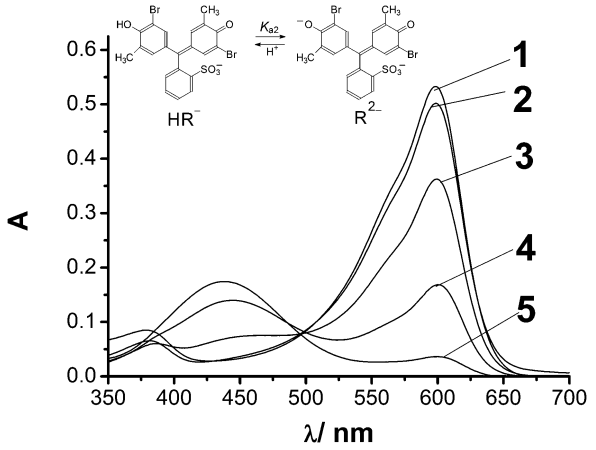

Fig. 12 The spectra of the indicator bromocresol purple at different pH values in 0.024% ND: the spectrum of R^{2-} with small NaOH addition, well below CCC (1); without HCl additions (2); with HCl additives, pH = 4.10 (3), 3.59 (4), and 3.04 (5).

from yellow (HR^-) to blue or purple (R^{2-}) and thus may be considered as one-color indicators in the region of around 600 nm (Fig. 12). Similar data for bromocresol purple and other indicator dyes in cationic surfactant micelles have been considered in a recent paper.[74] The limiting absorption of the basic forms may be measured just in the colloid solution without any additives: the pH value of the 0.024% hydrosol is *ca.* 6.2 (see ESI†). This ND concentration was chosen for more detailed examination. In some cases, very small amounts of NaOH, well below the CCC value, were added to ensure the complete transformation into R^{2-}.

The pK_a^{app} values are shown in Table 3. The pH values of the HCl solutions are 0.02 to 0.10 higher in the presence of the colloidal species, especially at high ND concentrations, up to 0.67%. Hence, some amount of acid is consumed for the protonation of the ND interfacial basic centers. The next difficulty for Ψ estimations was the uncertainty of the pK_a^i values. In the case of ionic surfactant micelles, the pK_a^i value of a given indicator is usually equated to its pK_a^{app} in micelle non-ionic surfactants, where $\Psi = 0$; otherwise, some more complicated algorithms are used.[72] In order to evaluate the polarity of the ND/water interface, we used two solvatochromic dyes, namely methyl orange and Reichardt's betaine. On going from water to the cationic surfactant micelles, these probes demonstrate expressed hypso- and bathochromic shifts of the absorption bands, respectively. In the case of the ND hydrosol, however, the above dyes exhibit but small band shifts against their spectra in water (see ESI†). This observation allows concluding that the ND surface is well-hydrated. Therefore, the pK_a^i value may be taken to be equal to the value in water, pK_a^w. Thus determined Ψ values are presented in Table 3. If pK_a^{app} in non-ionic micelles[72,73] are utilized as pK_a^i in eqn (4), the Ψ values come out about 50–60 mV higher.

Though the average value $\Psi = +139 \pm 27$ mV is only a rough estimate, it looks out noncontradictory, because the experimentally measured ζ values are at least twice lower within the whole ND concentration range, *e.g.*, $\zeta = +51.9 \pm 2.8$ mV and $+62.2 \pm 0.8$ for 2.9 and 0.036% ND solutions, respectively. Though the acid probably protonates some interfacial basic centers of ND species (see above), the general decrease in the average Ψ from +176 to +111 along with the increase in HCl concentration from 0.1 to 1.0 mM reflects the screening of the interfacial charge.

Of course, in agreement with the theory of the double electrical layer the Ψ values must be higher as compared with those of ζ. But in our case, the differences are too large. Upon studying the dyes bromocresol green and bromophenol blue associated with micelles of cationic surfactants, Mukerjee and Banerjee deduced the Ψ values much closer to ζ.[75]

As dyes are normally situated in the Stern region of the interfaces,[72] the Ψ value should be higher as compared with that of the electrokinetic potential.[76,77] In the present study, the Ψ:ζ ratio appeared to be 2.6 to 2.8, at equal bulk ionic strength. This may be explained by the proximity of the Ψ value rather to that of the inner Helmholtz plane, Ψ_0, than to the Ψ_d value of the outer plane. Using other formulae instead of Smoluchowski's for ζ calculation does not change the situation principally. Note that high Ψ_0 values, close to ours Ψ, have been determined under similar conditions using an absolutely different experimental method, for larger ND species of another origin.[25]

On the other hand, taking into account that the TEM images give no evidence of tight spherical shapes of the ND secondary aggregates, which are probably porous, the determined Ψ values may reflect rather the local electrostatic potential in the region where the indicator dye is situated on the non-uniform ND interface. In turn, the local positive charges of the primary particles, as revealed *via* electrophoresis measurements, counteract in the tight association in the secondary aggregates.

Using eqn (33) from ref. 72, one may find that the $pK_a^{app} = 2.35$ for bromophenol blue (Table 3) refers to that in micelles of cetyltrimethylammonium chloride at the bulk equilibrium concentration of $[Cl^-] = 0.031$ M. In turn, at $[Cl^-] = 0.001$ M (Table 3), the pK_a^{app} in the mentioned surfactant micelles should be as low as 1.26.

4.7 The application of the DLVO theory

This theory allows estimating the electrostatic repulsion energy U_{el} and the attractive energy U_{attr} of dispersion interaction between two spheres with radii r.[58–61] The primary 3 nm particles are evidently too small to be described by the DLVO theory in its classical version.[78,79] Hence, only the secondary aggregates should be considered. Also, judging the TEM images of the dried samples, the species may be considered to be spherical only for approximate estimates.

As the condition $\Psi_d \ll 26$ mV is not fulfilled for the system under study, the more general expression for U_{el} proposed by Dukhin *et al.*[80] was chosen for numerical estimates:

$$U = U_{el} + U_{attr} = 64\pi\varepsilon_r\varepsilon_0\left(\frac{RT}{F}\right)^2 \mathrm{tgh}^2\left(\frac{\Psi_d F}{4RT}\right)\frac{r\exp(-\kappa h)}{s} - \frac{A_{DWD}^*}{6}\left[\frac{2}{s^2-4}+\frac{2}{s^2}+\ln\frac{s^2-4}{s^2}\right] \quad (7)$$

Published on 27 May 2015. Downloaded by University of California - San Diego on 02/06/2015 16:29:49.

Table 3 The indices of the apparent ionization constants of the acid–base indicators, pK_a^{app}, and the estimates of the interfacial electrical potential, Ψ, in 0.024% ND sol

	c(HCl) × 10^4/M				
	10.00	5.01	3.16	2.00	1.00
Indicators	pK_a^{app} [a] (Ψ/mV)				
Bromophenol blue [4.20][b]	2.35 (109)	—	—	—	—
Bromocresol green [4.90][b]	3.38 (90)	3.37 (90)	3.34 (92)	3.27 (96)	—
Bromocresol purple [6.40][b]	4.13 (134)	—	3.81 (153)	—	3.58 (167)
Sulfonefluorescein [6.76][b]	—	3.96 (166)	3.54 (190)	3.56 (189)	3.62 (186)
Average Ψ/mV	111	128	145	142	176

[a] 25 °C. [b] In the brackets, the pK_a^w values in water are given.

Here, $\varepsilon_0 = 8.854 \times 10^{-12}$ F m^{-1}, the relative permittivity ε_r = 78.4 at T = 298.15 K, κ is the reciprocal Debye length, $s = 2 + h/r$, and h is the inter-particle distance. Eqn (7) is chosen also because the r and h values are commensurable. The A_{DWD}* constant may be calculated by the well-known formula:

$$A_{DWD}^{*} = (A_{DD}^{1/2} - A_{WW}^{1/2})^2. \quad (8)$$

Here A_{DD} and A_{WW} stand for the Hamaker constants of the diamond and water, respectively. According to Visser,[81] A_{DD} = 28.4 × 10^{-20} J and A_{WW} = 2.5 × 10^{-20} J, therefore, A_{DWD}* = 1.40 × 10^{-19} J. Israelachvili[82] gave the values of A_{DD} = (28.9–29.6) × 10^{-20} J and A_{WW} = (3.7–5.5) × 10^{-20} J, which resulted in A_{DWD}* = 1.1 × 10^{-19} J, if the average values of Hamaker constants are used. Selecting the values A_{DD} = 28.9 × 10^{-20} J and A_{WW} = 3.7 × 10^{-20} J, calculated *via* eqn (13.16) in ref. 82, one obtains A_{DWD}* = 1.2 × 10^{-19} J. We used this value in further calculations.

The next problem is the choice of the Ψ_d value. The Ψ values have been estimated above using the acid–base indicators, but they may be in fact local electrostatic potentials and describe rather the specific positions of these large organic ions in the porous secondary aggregates. On the other hand, relatively low ζ values may be considered as Ψ_d at the given κ value. We used both Ψ values determined using indicators and the experimentally measured zeta values in order to compare thus obtained Hamaker diagrams with the CCC data.

In the first case, using the Ψ = 111 mV value at 0.001 M HCl (Table 3), the interfacial charge density, q_s, was calculated for r = 15 nm (a typical value for diluted ND solutions, from DLS data) and κ = 0.104 nm^{-1} by Ohshima–Healy–White eqn (9) for spherical particles.[83]

$$q_s = \frac{2\varepsilon\varepsilon_0\kappa RT}{F}\sinh\left(\frac{\Psi F}{2RT}\right) \times \left(1 + \frac{2}{\kappa r\cosh^2(\Psi F/4RT)} + \frac{8\ln[\cosh(\Psi F/4RT)]}{(\kappa r)^2\sinh^2(\Psi F/2RT)}\right)^{1/2} \quad (9)$$

Then the same equation was used for the calculation of Ψ at different ionic strengths, *i.e.*, NaCl concentrations, considering q_s as a constant parameter. The series of U *vs.* h dependencies for varying ionic strength are presented in Fig. 13a. Alternatively, in Fig. 13b the curves calculated using the ζ values in eqn (7) as measured at the corresponding NaCl concentrations are shown.

Whereas the first approach demonstrates a substantially high potential barrier even at 10 mM NaCl, the second one is in line with the experimentally determined CCC value of 2.8 mM NaCl, because the coagulation becomes probable if U accounts for several k_BT units. This is in line with the recommendation to use the ζ value as Ψ_d in the DLVO calculations.[69]

Alternatively, it may be supposed that Ψ_d substantially exceeds ζ, but some additional factors, such as IICI attraction between the facets possessing negative and positive electrostatic potential[28,29] as well as hydrophobic interactions and some others,[84] not included in eqn (7) are of significance here.

For hydrophobic or multi-charged anions, the additional decrease in Ψ due to adsorption becomes very probable.

4.8 Coagulation by anionic surfactants

Though the tail length of anionic surfactants plays some role, thus revealing the adsorption of these anions on the positive ND surface, the effect is much weaker than expected resulting from their surface activity. Indeed, the last-named increases, in accordance with the Duclaux–Traube rule, (3–3.5)-fold with lengthening of the hydrocarbon tail by one CH_2 group.[66,85,86] Due to the same reason, the critical micelle concentration decreases two-fold.[66,86] The CCC values of ionic surfactants depend on their ability to be adsorbed on the colloidal particles in line with the above rule.[66,67] In the case of ND, however, the CCC decreases only 4 times on going from C_8 to the long-tailed surfactant anions, whereas the CCC values for C_{12}, C_{14}, and C_{16} are statistically indistinguishable (Table 2). Such a phenomenon is usually connected with the limitations of long tail adsorption in pores.[86] (Note that the second (tail-to-tail) stabilizing layer is not typical for the ND hydrosol under study.) The reported porous character of the ND aggregates[24,49] was already mentioned in the Introduction. The pores may appear in the secondary aggregates formed by primary species, for instance, because the fractal structure of the aggregates is possible.[18,22] Therefore, though the hydrocarbon portions of the surfactants favor the hydrophobization of the ND/water interface, the attachment of too long tails faces steric difficulties. Otherwise, it deals with a critical interfacial charge density causing coagulation, which is already reached by the adsorption of alkyl sulfates (sulfonates) with a medium tail length.

Published on 27 May 2015. Downloaded by University of California - San Diego on 02/06/2015 16:29:49.

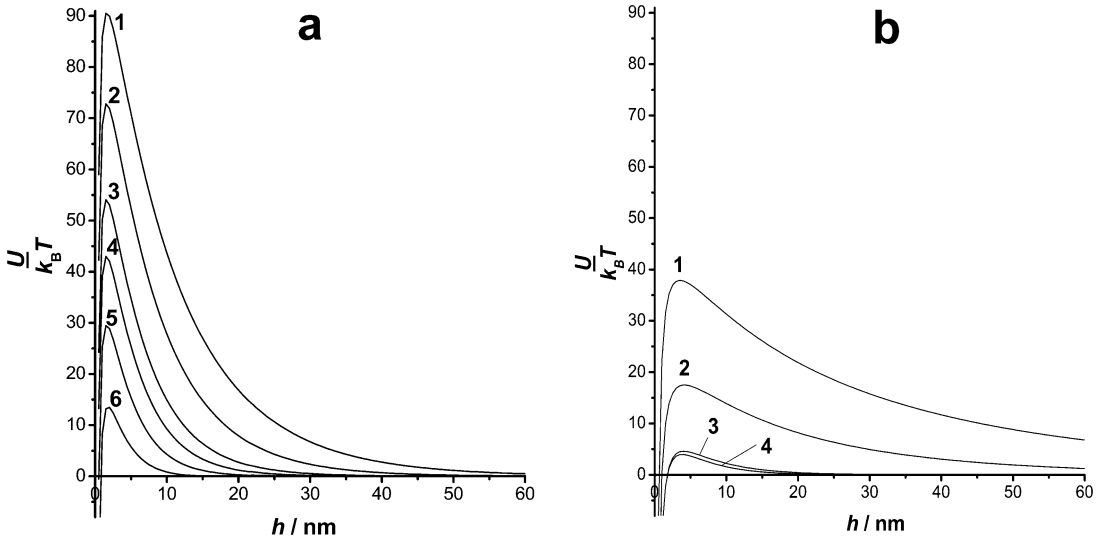

Fig. 13 Hamaker diagrams for the ND hydrosol at ionic strengths of 0.5 mM (1); 1.0 (2); 2.0 (3); 3.0 (4); 5.0 (5); and 10.0 mM NaCl (6), using the Ψ = 111 mV value at κ = 0.104 nm^{-1} and eqn (9) for calculating other Ψ values (a) and at ionic strengths of 0.02 mM (1); 0.1 (2); 2.0 (3); and 3.0 mM NaCl (4), with ζ = 62.2, 43.3, 32.4, and 33.2 mV, respectively, using instead of Ψ_d in eqn (7) (b).

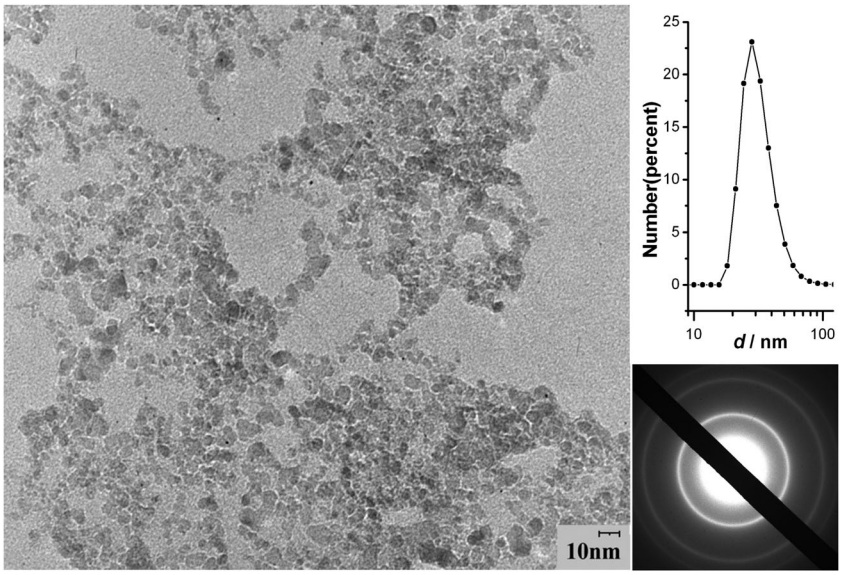

Fig. 14 The TEM image and the selected area electron diffraction pattern of the 0.036% ND hydrosol after evaporation of water (see also Section 4.1); top right corner: the particle size distribution by number in 0.03% sol, as determined by the DLS method.

Despite the porosity and the (probable) loose structure of the aggregates, the primary particles are rather firmly fixed therein. For instance, the sonication (electrical power *ca.* 50 W) for 25 min of the 0.027% ND hydrosol with an average size of 30 nm and PDI = 0.180 resulted in the average particle size of 18 nm and some fraction of micron species, PDI = 0.312. The primary 3 nm particles do not appear after such a light treatment.

4.9 The concentration-dependent properties of the ND hydrosol

The data depicted in Fig. 1 clearly show that the number of small particles around 3 nm decreases with dilution; the DLS data exemplified in Fig. 14 prove the reproducibility of the results.

The above-discussed porosity of the species at 0.19% supports the hypothesis of formation of secondary aggregates at lower ND concentrations. The TEM images give more definite evidence; the results typified in Fig. 14 are representative examples of a much larger body of data for both 0.036 and 0.0036% ND (see ESI†).

A qualitatively similar picture was obtained using SLS. At the same time, the increase in the particle size is accompanied by the drop of the viscosity (Fig. 15). Similar viscosity data have been already reported for ND hydrosols.[26] The differences in

 This journal is © the Owner Societies 2015

Published on 27 May 2015. Downloaded by University of California - San Diego on 02/06/2015 16:29:49.

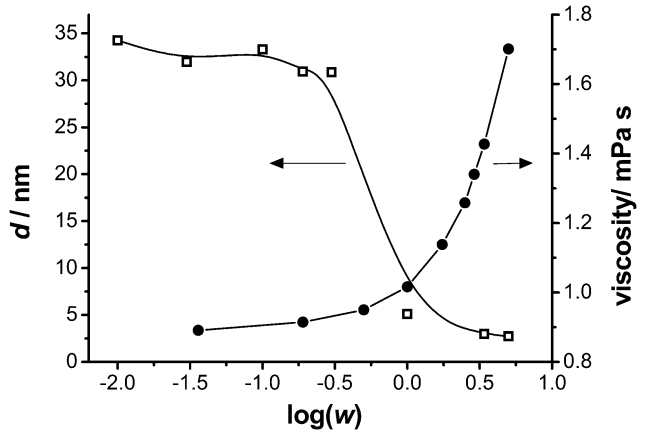

Fig. 15 The dependencies of the particle size (left) and viscosity (right) on the ND hydrosol concentration (logarithmic scale).

size manifest themselves even more distinctly under coagulation. About the CCC value, in the 3.0 mM NaCl solutions, the average sizes of 0.67%, 0.13%, and 0.024% ND hydrosols are 60, 87, and 244 nm, respectively, as determined by the DLS measurements. It should also be reminded that the apparent absorptivity increases along with dilution too (Fig. 3, inset).

It should be noted that more often the reverse process, *i.e.*, the dissociation of the secondary aggregates along with dilution takes place in colloid systems. For instance, the theory of coagulation proposed by Muller[58,59] explains the increase in CCC on going from concentrated to diluted sols using the concept of disaggregation of larger species. This theory appeared to be helpful for understanding the CCC values for the C_{60} hydrosols.[87]

For the ND hydrosols under study, the picture is reverse within the range of 0.01 to 5.0%. At this stage of research, we propose the following explanation. In concentrated solutions, the small particles interact through the surrounding water layers and form a class of so-called periodic colloid structures,[60,61,78] or "colloidal crystals",[88–93] which lead to some structuring of the sol and viscosity enhancement. Note that at 12 wt/vol%, the system converts into a hydrogel. In the 5 wt/vol% hydrosol, when the volume fraction of the dispersed matter is as small as 1.6%, the system is already on the way to gelation. Then, if the ND species are distributed uniformly, the average distance between the positively charged 2.7 nm-sized particles is about 10 nm. However, in the concentrated ND hydrosol, the zones of periodic colloidal structure do not necessarily cover the whole solution. In such a case, the rest of the solution may be considered as "voids".[90] For similar concentrated ND colloids, Avdeev *et al.*[18,94,95] deduced the presence of fractal aggregates based on the SANS data. Our DLS experiments, however, indicate the existence of small particles in the concentrated ND sol (Fig. 1 and 15). In any case, a two-fold increase in the viscosity as compared with pure water (Fig. 15) should be explained in terms of some assembling of primary species, such as fractals, rod- or worm-like structures. Taking into account the DLS data, the concept of periodical structures proposed in the present work seems to be reasonable for further discussion.

After dilution, the distances between the particles became larger, and it becomes more preferable to form secondary aggregates, much more separated from each other in aqueous medium.

Though the DLVO theory is inapplicable for 3 nm-sized species,[79] and as a rule the periodic colloidal structures or colloid crystals are formed by much larger species, some analogy with the coagulation in the "distant minimum", without direct contact,[60,61] seems to be reasonable. If the concentrated hydrosol is rather "tight", and a balance between attraction and repulsion of the neighboring nanoparticles takes place, the proposed structure appears to be the most preferable one.

For such a kind of colloidal system, some peculiarities have been noticed long ago, mostly for much larger particles of the dispersed phase,[60,61,88–92] but also for 7 nm Au nanoparticles.[93] The most significant one is as follows: the "secondary" or "distant" minimum, resulting from the cooperative interactions, may be deeper as compared with that calculated from the interaction of two particles only. Namely, the fixation of particles without direct contact may take place even if the repulsive forces overcome the attractive ones. The structural forces may also hinder the aggregation. Small concentrations of the electrolyte may favor the fixation in the distant minimum, whereas elevated concentrations result in adherence of the species. Note that at least *ca.* 3 mM of Cl^- ions are already present in the entire 5.0% ND hydrosol, while adding NaCl results in coagulation of this sol at the same CCC $\approx$3 mM.

The polydispersity index, PDI, gradually decreases with dilution. For instance, these values are equal to 0.590 for 5% ND hydrosol, 0.523 for 1%, and 0.241 and 0.190 for 0.19% and 0.036% hydrosols, respectively. Probably, some numbers of very large islands of associated species are also present in concentrated sols, as it is demonstrated by the DLS measurements in the volume-size and intensity-size distributions.

Upon dilution accompanied by stirring of the system, the cooperative interactions become weaker; the entropy factor ($\Delta S > 0$) favors uniform distribution of species in the enlarged volume. This results in destroying of such a quasi-equilibrated state, and the (probably stepwise) aggregation takes place owing to the hydrophobic interactions and van der Waals (dispersive) forces (Fig. 16). Instead of the network of small particles, larger aggregates are formed as a result of tight interaction between several neighboring primary particles.

Then further aggregation, or coagulation, becomes hindered by the lower probability of particle collision, the Brownian motion, and the decrease in the ionic concentration in the bulk and thus expansion of the diffuse parts of the double electrical layers of the ND aggregates.

Interestingly, the concentrated ND sols are inclined to very slow aging. Storing of the initial hydrosol for a period of time leads to some decrease in the viscosity (compare Fig. 15 and the data in Table 1). Also, the average particle size in the 2.9 and 2.5% ND sols determined by DLS two months later than that depicted in Fig. 15 exhibits an increase: d = 5.7 and 6.9 nm, respectively, which exceeds by 12–35% than that of 1.0% determined earlier. These and other similar observations denote the slight aggregation processes even in the concentrated ND solutions.

Published on 27 May 2015. Downloaded by University of California - San Diego on 02/06/2015 16:29:49.

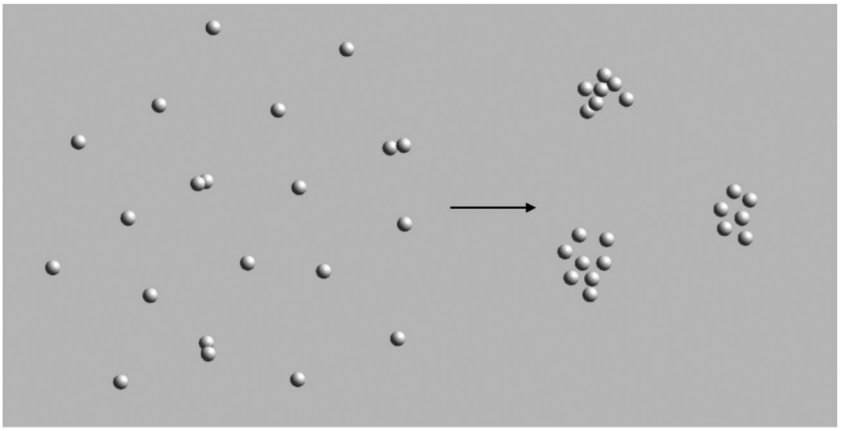

Fig. 16 The schematic picture of the dilution of the periodic structure resulting in the formation of larger colloidal aggregates.

5. Conclusions

Together with the non-diamond layer, the size of the colloidal species is 2.8 ± 0.6 nm. The light absorption decreases gradually from 350 to 700 nm, and the solutions do not obey the Bouguer–Lambert–Beer law. The fluorescence maximum is at 625 nm, while the emission excitation maximum is at 491 nm, just near the line of the argon-ion laser. The zeta-potential varies within the range of *ca.* +(40 to 60) mV depending on the ND concentration. Anionic dyes, such as bromophenol blue, rose Bengal B and other oxyxanthenes, are readily adsorbed on the colloidal species, which results in bathochromic shifts of the absorption bands of the dyes.

The coagulation points, CCC, were determined with nine inorganic electrolytes and five colloidal ionic surfactants using the procedure of spectrophotometric titration. These data are in line with the positive charge of the colloidal species. Indeed, the Schulze–Hardy rule predicts the sharp increase in the coagulation power of multi-charged anions in the case of "positive" sols. The fulfillment of the lyotropic (Hofmeister) series was also observed for single-charged anions. A cationic surfactant coagulates the hydrosol as a usual salt, the zwitter-ionic one does not exhibit any influence, whereas a set of alkyl sulfonates and sulfates displays expressed coagulative action thus revealing the adsorption/neutralization mechanism. The acidic nature of the positive charge of nanodiamond species becomes evident as follows from the abnormally low CCC value for NaOH and the elevated value for HCl. The potentiometric titrations confirm this finding.

The relatively weak coagulating power of hydrogen chloride allowed applying four acid–base indicators for examining the ND/water interface. Within the narrow pH range, the indices of the apparent ionization constants of the indicators, pK_a^{app}, were determined. This, in turn, opened up the possibility for estimating the interfacial electrical potential of the nanodiamond particles, Ψ. The last value was always higher as compared with that of the zeta-potential, in agreement with the principles of colloid chemistry.

The colloidal system under study exhibits unusual changes along with dilution from 5.00% up to 0.01%. The number of small particles around 3 nm decreases, whereas the average size turns to 30–35 nm. These DLS data are in line with the TEM images. The phenomenon may be explained in the following manner. In concentrated solutions, the small particles interact through the surrounding water layers and form a class of so-called periodic colloidal structures (colloidal crystals), which lead to some structuring of the sol and viscosity enhancement. The well-hydrated small particles interact through the surrounding water layers. This results in the formation of a structure resembling a closely packed crystal lattice. After dilution, the distances between the particles became larger, and it becomes more preferable to form secondary aggregates, much more separated from each other in aqueous medium.

Acknowledgements

We are grateful to our colleagues from Kharkov V. Karazin, National University: Sergey T. Goga for the determination of the electrical conductance and viscosity, Dr Alexander D. Roshal for fluorescence measurements, Dr Dmitriy Yu. Filatov and Dr D. S. Sofronov, Division of Functional Materials Chemistry, Institute for Single Crystals, National Academy of Science of Ukraine for IR measurements, and also Ekaterina Vus for measurements using the Zetasizer Nano ZS Malvern Instruments in Aalto University, Espoo, Finland. We also express our gratitude to Professor Paavo Kinnunen, Department of Biomedical Engineering and computational science, Aalto University, Espoo, Finland, for putting to our disposal the above-mentioned apparatus, Elena A. Korosteleva, Pharmstandart-Biolik, Kharkov, Ukraine, for static light scattering measurements, Dr Artem Yu. Kulikov and Kharkov V. Karazin, National University and Professor Sergei N. Shtykov, Saratov State University, Russia for supplying us with some anionic surfactants, Dr Teimur Shakhverdov, St-Petersburg, for gifting the sample of pseudoisocyanine iodide, and Professor Christian Reichardt, Philipps University of Marburg, Germany, for donating the solvatochromic betaine dye.

 This journal is © the Owner Societies 2015

Published on 27 May 2015. Downloaded by University of California - San Diego on 02/06/2015 16:29:49.

References

1 K. B. Holt, C. Ziegler, D. J. Caruana, J. Zang, E. J. Millan-Barrios, J. Hu and J. S. Foord, *Phys. Chem. Chem. Phys.*, 2008, **10**, 303–310.
2 J.-C. Arnault, T. Petit, H. Girard, A. Chavanne, C. Gesset, M. Sennour and M. Chaigneau, *Phys. Chem. Chem. Phys.*, 2011, **13**, 11481–11487.
3 A. Krueger, *J. Mater. Chem.*, 2011, **21**, 12571–12578.
4 T. Petit, J. C. Arnault, H. A. Girard, M. Sennour, T. Y. Kang, C. L. Cheng and P. Bergonzo, *Nanoscale*, 2012, **4**, 6792–6799.
5 V. N. Mochalin, O. Shenderova, D. Ho and Y. Gogotsi, *Nat. Nanotechnol.*, 2012, **7**, 11–23.
6 O. A. Shenderova and D. M. Gruen, *Ultrananocrystalline Diamond: Synthesis, Properties and Applications (Second Edition)*, William Andrew Publishing, 2012.
7 E. Osawa, S. Sasaki and R. Yamanoi, in *Ultrananocrystalline Diamond (Second Edition)*, ed. D. M. Gruen and O. A. Shenderova, William Andrew Publishing, Oxford, 2012, pp. 165–179, DOI: 10.1016/B978-1-4377-3465-2.00006-2.
8 L. Y. Chang, E. Osawa and A. S. Barnard, *Nanoscale*, 2011, **3**, 958–962.
9 E. Osawa, in *Handbook of Advanced Ceramics (Second Edition)*, ed. S. Somiya, Academic Press, Oxford, 2013, pp. 89–102, DOI: 10.1016/B978-0-12-385469-8.00004-6.
10 A. Pentecost, S. Gour, V. Mochalin, I. Knoke and Y. Gogotsi, *ACS Appl. Mater. Interfaces*, 2010, **2**, 3289–3294.
11 E. Osawa and D. Ho, *J. Nucl. Med. Allied Sci.*, 2012, **2**, 31–40.
12 J. T. Paci, H. B. Man, B. Saha, D. Ho and G. C. Schatz, *J. Phys. Chem. C*, 2013, **117**, 17256–17267.
13 V. I. Korepanov, H. Witek, H. Okajima, E. Ōsawa and H. Hamaguchi, *J. Chem. Phys.*, 2014, **140**, 04110711.
14 V. I. Korepanov, private communication.
15 O. A. Williams, J. Hees, C. Dieker, W. Jäger, L. Kirste and C. E. Nebel, *ACS Nano*, 2010, **4**, 4824–4830.
16 J. Hees, A. Kriele and O. A. Williams, *Chem. Phys. Lett.*, 2011, **509**, 12–15.
17 O. Shenderova, S. Hens and G. McGuire, *Diamond Relat. Mater.*, 2010, **19**, 260–267.
18 M. V. Avdeev, N. N. Rozhkova, V. L. Aksenov, V. M. Garamus, R. Willumeit and E. Ōsawa, *J. Phys. Chem. C*, 2009, **113**, 9473–9479.
19 M. Ozawa, M. Inaguma, M. Takahashi, F. Kataoka, A. Krüger and E. Ōsawa, *Adv. Mater.*, 2007, **19**, 1201–1206.
20 N. Gibson, O. Shenderova, T. J. M. Luo, S. Moseenkov, V. Bondar, A. Puzyr, K. Purtov, Z. Fitzgerald and D. W. Brenner, *Diamond Relat. Mater.*, 2009, **18**, 620–626.
21 N. Gibson, T.-J. Luo, O. Shenderova, A. Koscheev and D. Brenner, *J. Nanopart. Res.*, 2012, **14**, 1–12.
22 F. Gareeva, N. Petrova, O. Shenderova and A. Zhukov, *Colloids Surf., A*, 2014, **440**, 202–207.
23 C. Desai, K. Chen and S. Mitra, *Environ. Sci.: Processes Impacts*, 2014, **16**, 518–523.
24 N. Petrova, A. Zhukov, F. Gareeva, A. Koscheev, I. Petrov and O. Shenderova, *Diamond Relat. Mater.*, 2012, **30**, 62–69.
25 A. N. Zhukov, F. R. Gareeva and A. E. Aleksenskii, *Colloid J.*, 2012, **74**, 463–471.
26 A. Y. Vul, E. D. Eydelman, M. Inakuma and E. Ōsawa, *Diamond Relat. Mater.*, 2007, **16**, 2023–2028.
27 N. M. Gibson, T. J. M. Luo, O. Shenderova, Y. J. Choi, Z. Fitzgerald and D. W. Brenner, *Diamond Relat. Mater.*, 2010, **19**, 234–237.
28 A. S. Barnard, *J. Mater. Chem.*, 2008, **18**, 4038–4041.
29 A. S. Barnard and E. Osawa, *Nanoscale*, 2014, **6**, 1188–1194.
30 A. S. Barnard and M. Sternberg, *J. Mater. Chem.*, 2007, **17**, 4811–4819.
31 T. Jiang and K. Xu, *Carbon*, 1995, **33**, 1663–1671.
32 T. Jiang, K. Xu and S. Ji, *J. Chem. Soc., Faraday Trans.*, 1996, **92**, 3401–3406.
33 S. Ji, T. Jiang, K. Xu and S. Li, *Appl. Surf. Sci.*, 1998, **133**, 231–238.
34 E. Mironov, A. Koretz and E. Petrov, *Diamond Relat. Mater.*, 2002, **11**, 872–876.
35 I. I. Kulakova, *Phys. Solid State*, 2004, **46**, 636–643.
36 X. Xu, Z. Yu, Y. Zhu and B. Wang, *Diamond Relat. Mater.*, 2005, **14**, 206–212.
37 O. Shenderova, I. Petrov, J. Walsh, V. Grichko, V. Grishko, T. Tyler and G. Cunningham, *Diamond Relat. Mater.*, 2006, **15**, 1799–1803.
38 V. Mochalin, S. Osswald and Y. Gogotsi, *Chem. Mater.*, 2009, **21**, 273–279.
39 H. B. Man, H. Kim, H.-J. Kim, E. Robinson, W. K. Liu, E. K.-H. Chow and D. Ho, *Nanomedicine*, 2014, **10**, 359–369.
40 A. Krüger, F. Kataoka, M. Ozawa, T. Fujino, Y. Suzuki, A. E. Aleksenskii, A. Y. Vul' and E. Ōsawa, *Carbon*, 2005, **43**, 1722–1730.
41 O. Shenderova, A. M. Panich, S. Moseenkov, S. C. Hens, V. Kuznetsov and H. M. Vieth, *J. Phys. Chem. C*, 2011, **115**, 19005–19011.
42 M. V. Korobov, D. S. Volkov, N. V. Avramenko, L. A. Belyaeva, P. I. Semenyuk and M. A. Proskurnin, *Nanoscale*, 2013, **5**, 1529–1536.
43 Z. Wang, C. Xu and C. Liu, *J. Mater. Chem. C*, 2013, **1**, 6630–6636.
44 W. Peng, R. Mahfouz, J. Pan, Y. Hou, P. M. Beaujuge and O. M. Bakr, *Nanoscale*, 2013, **5**, 5017–5026.
45 A. T. Collins and G. S. Woods, *Philos. Mag. B*, 1982, **46**, 77–83.
46 V. N. Mochalin, S. Osswald, C. Portet, G. Yushin, C. Hobson, M. Havel and Y. Gogotsi, *MRS Online Proc. Libr.*, 2007, **1039**, DOI: 10.1557/PROC-1039-P11-03.
47 E. V. Basiuk, A. Santamaría-Bonfil, V. Meza-Laguna, T. Y. Gromovoy, E. Alvares-Zauco, F. F. Contreras-Torres, J. Rizo, G. Zavala and V. A. Basiuk, *Appl. Surf. Sci.*, 2013, **275**, 324–334.
48 V. N. Mochalin, I. Neitzel, B. J. M. Etzold, A. Peterson, G. Palmese and Y. Gogotsi, *ACS Nano*, 2011, **5**, 7494–7502.
49 A. E. Aleksenskiy, E. D. Eydelman and A. Y. Vul, *Nanosci. Nanotechnol. Lett.*, 2011, **3**, 68–74.
50 G. Taguchi, S. Chowdhury and Y. Wu, in *Taguchi's Quality Engineering Handbook*, John Wiley & Sons, Inc., 2007, pp. 56–123, DOI: 10.1002/9780470258354.ch4.
51 S. Sasaki, R. Yamanoi and E. Ōsawa, Dispersion of Detonation Nanodiamond: A Progress Report, presented before the

Published on 27 May 2015. Downloaded by University of California - San Diego on 02/06/2015 16:29:49.

46th Fullerenes-Nanotubes-Graphenes General Symposium, Oral 1-4, University of Tokyo, 2013, p. 12.
52 S. Gorelik, Y. Skakov and L. Rastorguev, *X-ray and Electron-Optical Analysis*, MISIS, Moscow, 2002.
53 A. Guinier, *X-ray Diffraction in Crystals, Imperfect Crystals, and Amorphous Bodies*, Courier Corporation, 1994.
54 F. P. Treadwell, *Analytical Chemistry*, J. Wiley & sons, inc., New York, 1916.
55 N. O. Mchedlov-Petrossyan, E. Y. Bryleva, N. A. Vodolazkaya, A. A. Dissanayake and W. T. Ford, *Langmuir*, 2008, **24**, 5689–5699.
56 N. O. Mchedlov-Petrossyan, N. A. Vodolazkaya, R. V. Rodik, L. N. Bogdanova, T. A. Cheipesh, O. Y. Soboleva, A. P. Kryshtal, L. V. Kutuzova and V. I. Kalchenko, *J. Phys. Chem. C*, 2012, **116**, 10245–10259.
57 B. Derjaguin and L. Landau, *Zh. Eksp. Theoret. Fiz.*, 1945, **15**, 663–682.
58 B. V. Derjaguin, *The Theory of Stability of Colloids and Thin Films*, Nauka, Moscow, 1986.
59 B. V. Derjaguin, N. V. Churaev and V. M. Muller, *Interfacial Forces*, Nauka, Moscow, 1985.
60 I. F. Efremov and O. G. Us'yarov, *Russ. Chem. Rev.*, 1976, **45**, 435–453.
61 H. Sonntag, K. Strenge and B. Vincent, *Coagulation Kinetics*, Springer US, 1987.
62 T. Oncsik, G. Trefalt, Z. Csendes, I. Szilagyi and M. Borkovec, *Langmuir*, 2014, **30**, 733–741.
63 M. Sano, J. Okamura and S. Shinkai, *Langmuir*, 2001, **17**, 7172–7173.
64 N. O. Mchedlov-Petrossyan, V. K. Klochkov and G. V. Andrievsky, *J. Chem. Soc., Faraday Trans.*, 1997, **93**, 4343–4346.
65 L.-Q. Zhang, Y.-K. Zhang, X.-C. Lin, K. Yang and D.-H. Lin, *J. Zhejiang Univ., Sci., A*, 2014, **15**, 634–642.
66 K. Shinoda, T. Nakagawa, B.-I. Tamamushi and T. Isemura, *Colloidal Surfactants (Russ. transl.)*, Mir, Moscow, 1966.
67 K. Inoue, A. Kitahara, S. Koseki and A. B. Hachoyan, *Interface Chemistry (Russian transl.)*, Mir, Moscow, 1983.
68 J. Lyklema, *J. Colloid Interface Sci.*, 2013, **392**, 102–104.
69 J. Lyklema, *Colloids Surf., A*, 2014, **460**, 468–472.
70 C. A. Leon y Leon, J. M. Solar, V. Calemma and L. R. Radovic, *Carbon*, 1992, **30**, 797–811.
71 F. Grieser and C. J. Drummond, *J. Phys. Chem.*, 1988, **92**, 5580–5593.
72 N. O. Mchedlov-Petrossyan, *Pure Appl. Chem.*, 2008, **80**, 1459–1510.
73 N. O. Mchedlov-Petrossyan, N. A. Vodolazkaya and N. N. Kamneva, in *Micelles: Structural Biochemistry, Formation and Functions & Usage*, ed. D. Bradburn and T. Bittinger, Nova Science Pub Inc, New York, 2013, ch. 1, pp. 1–72.
74 N. N. Kamneva, A. Y. Kharchenko, O. S. Bykova, A. V. Sundenko and N. O. Mchedlov-Petrossyan, *J. Mol. Liq.*, 2014, **199**, 376–384.
75 P. Mukerjee and K. Banerjee, *J. Phys. Chem.*, 1964, **68**, 3567–3574.
76 J. Lyklema, *J. Colloid Interface Sci.*, 1977, **58**, 242–250.
77 J. Lyklema, *Colloids Surf., A*, 2011, **376**, 2–8.
78 B. V. Deryagin, *Russ. Chem. Rev.*, 1979, **48**, 363–388.
79 L. B. Boinovich, *Russ. Chem. Rev.*, 2007, **76**, 471.
80 S. S. Dukhin, B. V. Drejaguin and N. M. Semenikhin, *Doklady AN USSR*, 1970, **192**, 357–360.
81 J. Visser, *Adv. Colloid Interface Sci.*, 1972, **3**, 331–363.
82 J. N. Israelachvili, *Intermolecular and surface forces: revised third edition*, Academic press, 2011.
83 H. Ohshima, T. W. Healy and L. R. White, *J. Colloid Interface Sci.*, 1982, **90**, 17–26.
84 L. Lai and A. S. Barnard, *J. Phys. Chem. Lett.*, 2012, **3**, 896–901.
85 A. W. Adamson, *Physical Chemistry of Surfaces, (Russ. transl.)*, Mir, Moscow, 1979.
86 D. A. Fridrikhsberg, *The Course of Colloid Chemistry. (In Russian)*, Khimiya, Leningrad, 1984.
87 N. O. Mchedlov-Petrossyan, *Chem. Rev.*, 2013, **113**, 5149–5193.
88 P. N. Pusey and W. van Megen, *Nature*, 1986, **320**, 340–342.
89 J. W. Goodwin and R. H. Ottewill, *J. Chem. Soc., Faraday Trans.*, 1991, **87**, 357–369.
90 K. Ito, H. Yoshida and N. Ise, *Science*, 1994, **263**, 66–68.
91 A. Rugge, W. T. Ford and S. H. Tolbert, *Langmuir*, 2003, **19**, 7852–7861.
92 D. Qin, S. Tan, S. Qin and W. T. Ford, *Langmuir*, 2004, **20**, 3145–3150.
93 J. Zhou, J. Ralston, R. Sedev and D. A. Beattie, *J. Colloid Interface Sci.*, 2009, **331**, 251–262.
94 M. V. Avdeev, V. L. Aksenov, O. V. Tomchuk, L. A. Bulavin, V. M. Garamus and E. Osawa, *J. Phys.: Condens. Matter*, 2013, **25**, 445001.
95 O. V. Tomchuk, D. S. Volkov, L. A. Bulavin, A. V. Rogachev, M. A. Proskurnin, M. V. Korobov and M. V. Avdeev, *J. Phys. Chem. C*, 2015, **119**, 794–802.

 This journal is © the Owner Societies 2015